Chapter 10

The Catalytic Manganese Cluster: Organization of the Metal Ions

Vittal K. Yachandra*
Melvin Calvin Laboratory, Physical Biosciences Division, Lawrence Berkeley National Laboratory, Berkeley, CA 94720, U.S.A.

Summary

The light-induced oxidation of water to O_2 is catalyzed by a four-manganese atom cluster associated with Photosystem II (PS II). This chapter summarizes ongoing investigations of the oxidation state, the structure and the associated cofactors calcium and chloride of the catalytic Mn cluster using X-ray and electron paramagnetic resonance (EPR) spectroscopy. Manganese K-edge X-ray spectroscopy, Kβ X-ray emission spectroscopy (XES), and extended X-ray absorption fine structure (EXAFS) studies have not only determined the oxida-

---

*Email: VKYachandra@LBL.gov

T. Wydrzynski and K. Satoh (eds): Photosystem II: The Light-Driven Water:Plastoquinone Oxidoreductase, pp. 235–260.

tion states and structural features, but also changes that occur in oxidation state of the Mn cluster and in its structural organization during the accumulation of oxidizing equivalents leading to O_2 formation. Combining X-ray spectroscopy information with X-ray diffraction studies, and consistent with the available EPR data, we have succeeded in limiting the range of likely structures of the Mn cluster. EXAFS studies at the strontium and calcium K-edges have provided evidence that the catalytic center is a Mn/Ca heteronuclear complex. Based on the X-ray spectroscopy data, models for the structure and a mechanism for O_2 evolution are presented.

I. Introduction

Most of the O_2 in the atmosphere that supports life on earth is generated by plants, algae, and cyanobacteria by the photo-induced oxidation of water to dioxygen:

$$2H_2O \rightarrow O_2 + 4e^- + 4H^+ \qquad (1)$$

This reaction is catalyzed by a manganese/calcium complex (Mn_4Ca), which sequentially stores four oxidizing equivalents (i.e. the S_n states, where n = 0 – 4) that are used to oxidize two molecules of water to molecular oxygen (Kok et al., 1970; for a review, see Joliot, 2003). The Mn complex is part of the multiprotein Photosystem II (PS II) assembly (Chapters 3–6), which contains the reaction center involved in photosynthetic charge separation (Chapter 7) and an antenna complex of chlorophyll molecules (Chapter 2). The assembly also contains cytochrome b_{559} (Chapter 15) and a Fe-quinone electron acceptor complex (Chapter 8).

X-ray absorption spectroscopy (XAS) (Sauer et al., 1992; Robblee et al., 2001) and electron paramagnetic resonance (EPR) (Dismukes and Siderer, 1981; Messinger et al., 1997b; Britt et al., 2000) studies have emerged as the primary methods to provide structural and chemical information about the oxygen evolving complex (OEC) and devise a working model for its Mn cluster. XAS has been used to examine the structural environment of metal ions in many proteins (Cramer, 1988; Yachandra, 1995). The energy of the incoming X-ray photons and of the outgoing fluorescence is specific to the Mn atom; hence, other metals or the protein matrix normally co-purified with the OEC in a PS II preparation do not interfere. Element-specificity and applicability to non-crystalline samples have made X-ray spectroscopy a useful technique for probing the structure of the Mn complex in the complicated environment of PS II, which has many components such as non-heme iron, cytochrome, chlorophylls that interfere with other techniques. The structural studies can also be performed on crystals, or on frozen solutions and several of the S state intermediates mentioned above have been stabilized as frozen solutions and studied by X-ray spectroscopy. The different regions of the X-ray spectrum provide complementary information: X-ray absorption near edge spectroscopy (XANES) yield information about the oxidation states and site symmetry of the absorbing atom while extended X-ray absorption fine structure (EXAFS) is sensitive to distances, numbers, and atomic number of atoms around the absorbing atom. The more recently used technique of X-ray emission spectroscopy (XES) has also provided information regarding the identity of the oxidation states of Mn complex in the various S-states and the changes accompanying the S-state advance.

Critical questions related to the process of photosynthetic water oxidation are: (i) What are the oxidation state(s) and structural changes in the Mn complex as the OEC proceeds through the S-state cycle? and (ii) What is the mechanism by which four electrons are removed from two water molecules by the Mn complex to produce an O_2 molecule? Electron paramagnetic resonance (EPR) and X-ray spectroscopy studies and the interplay between these two methods have provided significant insights into the structure and the mechanism of the OEC. This chapter focuses on the application of X-ray spectroscopic techniques to resolve structural questions regarding the Mn cluster in the OEC, with emphasis on the results from our laboratory. Many excellent reviews are available for comprehensive surveys of the Mn complex and the OEC, EPR, and XAS literature (Debus, 1992; Rutherford et al., 1992; Britt, 1996;

Abbreviations: Chl – chlorophyll; <E> – 1st-moment value; EPR – electron paramagnetic resonance; EXAFS – extended X-ray absorption fine structure; FT – Fourier transform; IPE – inflection point energy; MLS – multiline EPR signal; Mn_4 – catalytic manganese cluster; OEC – oxygen evolving complex; PS II – Photosystem II; S_n – states of the OEC for n = 0, 1, 2, 3, or 4; XANES – X-ray absorption near edge spectroscopy; XAS – X-ray absorption spectroscopy; XES – X-ray emission spectroscopy; Y_D^{ox} – oxidized form of the redox active tyrosine on D2; $Y_Z^{\bullet}$ – oxidized form of the redox active tyrosine on D1

Yachandra et al., 1996, 2002; Penner-Hahn, 1998; Robblee et al., 2001).

II. Oxidation States of the Manganese

Two key questions for the understanding of photosynthetic water oxidation are: (i) do all four oxidizing equivalents necessary to oxidize water to O_2 accumulate on the four Mn ions of the OEC, or do some ligand-centered oxidations take place before the formation and release of O_2 during the $S_3 \rightarrow [S_4] \rightarrow S_0$ transition; and (ii) what are the oxidation state assignments for the Mn during S-state advancement. X-ray absorption and emission spectroscopy of Mn, along with EPR have provided answers to these two pivotal questions.

A. Manganese X-Ray Absorption Near Edge Spectroscopy (XANES)

X-ray absorption near-edge spectroscopy (XANES) is the most well-known of the X-ray techniques and has been extensively used to investigate the oxidation states of redox-active metals in metalloprotein active sites. XANES results from the excitation of a 1s electron (K-shell) to a higher, bound orbital (Fig. 1, *Left*). The higher the oxidation state of the metal, the more positive the overall charge of the atom, and higher energy is required to excite an electron out of an orbital (Shulman et al., 1976). The first formally allowed electric dipole transition is the 1s→4p transition. Due to the size of the 4p orbital, it overlaps with p-orbitals of the ligands, either through σ or π bonding. Consequently, this transition is sensitive to the oxidation state and the ligand environment of the metal. For certain symmetries around the metal, the formally electric-dipole forbidden 1s→3d transition can be observed (arrow points to it in Fig. 1, *Middle* which is expanded in the inset), occurring at a lower energy than the main edge transitions (Roe et al., 1984). This transition is due to mixing of metal 3d and 4p orbitals, and gives information about the ligand as well as about the oxidation state and symmetry of the metal complex (Westre et al., 1997). To increase the sensitivity of XANES, absorption is detected as an excitation spectrum by measuring the $K\alpha$ fluorescence (2p to 1s) of the Mn atoms (Jaklevic et al., 1977).

The pioneering application of Mn XANES to PS II was performed by Kirby et al. (1981) on chloroplasts and Goodin et al. (1984) on PS II preparations in the early 1980s. These studies, although extremely difficult because of the low Mn concentration, showed that the Mn K-edge from the S_2 state is shifted to higher energy relative to the Mn K-edge from the S_1 state. Dramatic improvements in detector technology and cryostat cooling capabilities have made XANES experiments practical using concentrated PS II preparations (McDermott et al., 1988; Guiles et al., 1990a; DeRose et al., 1994), and the collection of XANES spectra from dilute, single-flash saturable PS II samples is now achievable. Three different groups have investigated the oxidation states of Mn for the S_0, S_1, S_2, and S_3 states using XANES on single-flash saturable PS II samples. Based on shifts in the absorption edge, or lack thereof, Roelofs et al. (1996) proposed that Mn is oxidized during the $S_0 \rightarrow S_1$ and $S_1 \rightarrow S_2$ transitions, but is not oxidized during the $S_2 \rightarrow S_3$ transition. In contrast, Ono et al. (1992) and Iuzzolino et al. (1998) interpret their XANES results to indicate that Mn is oxidized during each S-state transition, although Ono et al. (1992) reported no independent S-state determination for their samples and Iuzzolino et al. (1998) had significant S-state inhomogeneity in their samples. However, improved XANES data for S-state transitions, have shown a Mn K-edge shift of only 0.4 eV for the S_2 to S_3 transition (Ono et al., 1994). The results of Roelofs et al (1996) indicating the absence of Mn centered oxidation during the S_2 to S_3 transition has been reproduced by Messinger et al. (2001) using both XANES (Fig. 1, *Middle* and *Right*) and Mn XES studies (see below).

B. Manganese Kβ X-Ray Emission Spectroscopy (XES)

The recent studies by Messinger et al. (2001) have combined EPR, XANES and XES studies to address the questions of oxidation state assignments and changes during the S state cycle. In contrast to XANES, Kβ XES detects the X-ray emission from the relaxation of a 3p electron to a 1s hole, which is created by excitation of a 1s electron into the continuum (Fig. 2, *Left*). In a simplified model, two final states exist due to a constructive ($K\beta_{1,3}$) or destructive ($K\beta'$) spin-exchange interaction between the unpaired electrons in the 3p and 3d orbitals (Tsutsumi et al., 1976). The magnitude of the exchange interaction depends on the number of unpaired electrons in the 3d orbital. In the high spin case, increasing the oxidation state of the metal decreases the number of

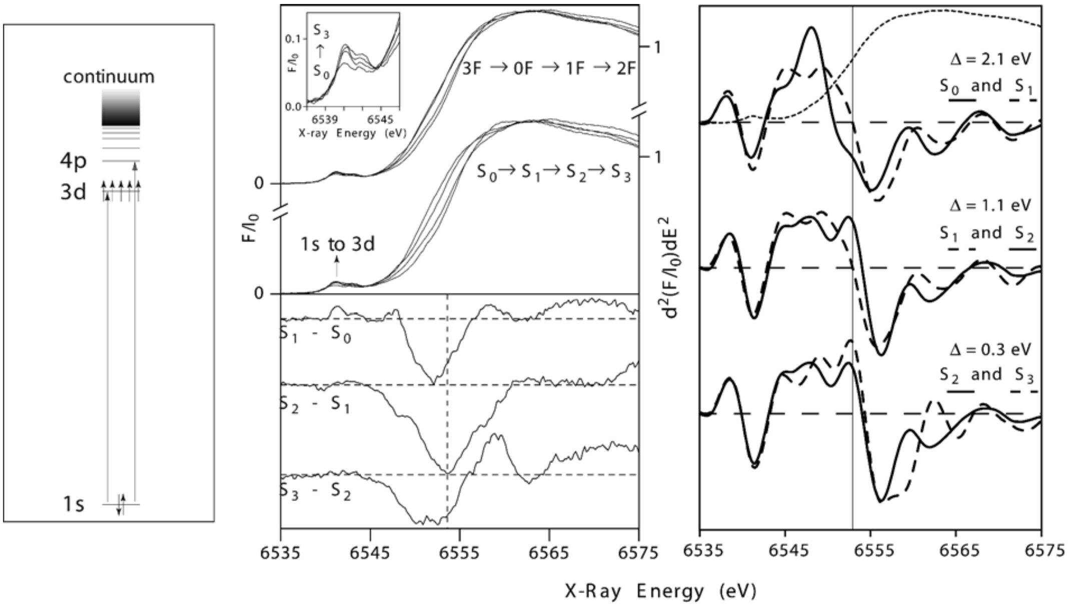

Fig. 1. Left. A schematic diagram for the excitation and emission processes involved in Mn XANES. The weak 1s to 3d transition is dipole-forbidden and the principal transition is from 1s to a molecular orbital with p character. To enhance sensitivity, the X-ray absorption spectra are collected as excitation spectra using Mn Kα (2p to 1s) fluorescence detection. *Middle Top*. Mn K-edge XANES spectra of flash-illuminated PS II samples. Pure S-state spectra (bottom) were obtained from the flash spectra (top) by deconvolution using multiline EPR spectra. The pre-edge region (principally a 1s → 3d transition) for the $S_0 – S_3$ states is shown in the inset. The inflection point energy (IPE) changes from S_0 to S_1 and S_1 to S_2 transitions are substantial but are much smaller for the S_2 to S_3 transition. *Middle Bottom*. S-state Mn XANES difference spectra show that each transition is unique. The horizontal dashed lines show the zero value for each difference spectrum. Adapted from Messinger et al. (2001) and Visser et al. (2001). *Right.* Second derivatives of the normalized, pure S-state Mn K-edge spectra of the Mn-cluster of PS II. For clarity a vertical dashed line has been drawn at the inflection point energy (IPE) of the S_1-state. The change in IPE (Δ in eV) for each S-state advance is given at the right shows the significant shifts for the S_0 to S_1 and S_1 to S_2 transitions but is much smaller for the S_2 to S_3 transition indicating that a Mn centered oxidation is unlikely for the S_2 to S_3 transition. For reference, the K-edge spectrum of the S_1-state is plotted as well (dashed line). Adapted from Messinger et al. (2001).

unpaired 3d electrons; concomitantly, the spin exchange interaction decreases. Accordingly, the $K\beta_{1,3}$ transition shifts to a higher and the Kβ′ transition shifts to a lower energy (Peng et al., 1994). Compared to the 4p orbitals, the 3p orbitals have less overlap with the ligand orbitals, because they are smaller and more buried within the electronic shells. Therefore, Kβ XES is less sensitive to the ligand environment compared to XANES. The $K\beta_{1,3}$ transition is better resolved than the Kβ′ transition due to a difference in relaxation processes. Hence, the $K\beta_{1,3}$ transition is used as a indicator of the oxidation state of the metal. A more accurate view on Kβ XES requires the ligand-field multiplet formalism. This indicates that there is some dependence of the ligand environment on Kβ XES spectra.

Shown in Fig. 2, *Middle*, and inset are the Kβ emission spectra of Mn(IV)O_2, Mn_2(III)O_3, and Mn(II)O, which illustrate the features of Kβ emission spectra and their sensitivity to the oxidation states of Mn. As the oxidation state of Mn increases from Mn(II) to Mn(III) to Mn(IV), fewer unpaired 3d valence electrons are available to interact with the 3p hole; thus, the magnitude of the 3p – 3d exchange interaction becomes smaller, leading to a decrease in the Kβ′ – $K\beta_{1,3}$ splitting. The consequence is that, if one focuses only on the more intense $K\beta_{1,3}$ emission peak, it shifts to lower energy as Mn is oxidized. Whereas the Kβ emission spectrum is sensitive to oxidation state through a 3p – 3d exchange interaction, the technique of XANES spectroscopy is sensitive to oxidation state through a different mechanism: core-hole shielding effects. This is why, upon Mn oxidation, $K\beta_{1,3}$ emission spectra shift to lower energy, while XANES

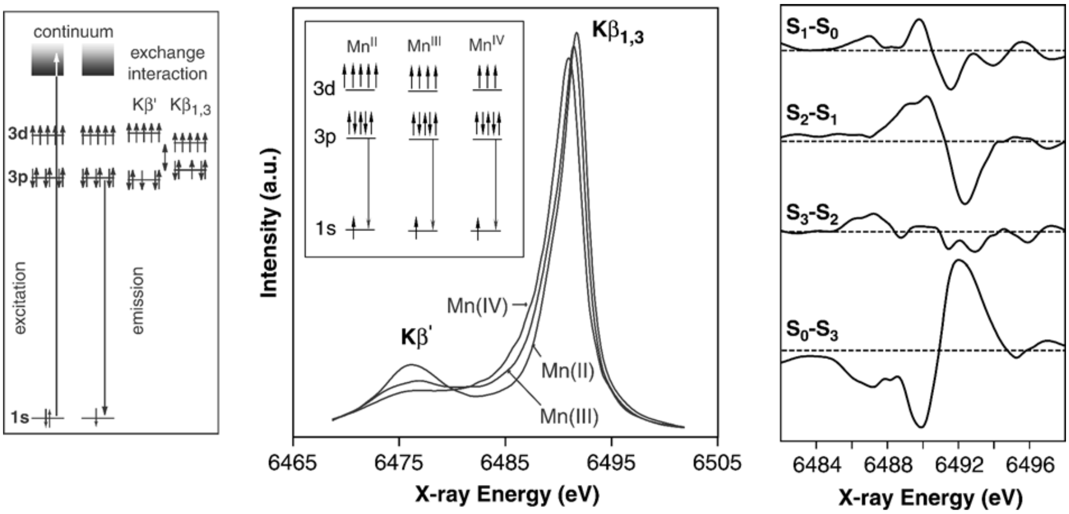

Fig. 2. Kβ spectra of Mn(II), (III) and (IV) oxides. *Left.* Energy level diagram showing the absorption (1s to continuum) and emission processes (3p to 1s) involved in Kβ Mn XES. In a simplified model, two final spin states exist with either a constructive (Kβ$_{1,3}$) or destructive (Kβ') spin exchange interaction between the unpaired 3p and 3d electrons. The magnitude of the interaction depends on the number of unpaired 3d electrons, which is related to the oxidation state of the metal. Adapted from Messinger et al. (2001) and Visser et al. (2001). *Middle.* Changes in the Kβ spectrum due to Mn oxidation. The inset shows a pictorial representation of the Kβ fluorescence transition for each of the oxides. Kβ XES arises from the emission of a 3p electron to 1s hole, which is formed following X-ray absorption. *Right.* The S$_1$-S$_0$, S$_2$-S$_1$, S$_3$-S$_2$ and S$_0$-S$_3$ difference high resolution Mn X-ray Kβ-emission spectra. The derivative shapes indicate shifts in the energy of the spectra between the S$_0$ and S$_1$, and S$_1$ and S$_2$ spectra, indicating oxidations of Mn. The S$_3$-S$_2$ difference spectra demonstrates the similarity of the spectra, suggesting that this advance does not involve a Mn centered oxidation. Adapted from Messinger et al. (2001).

spectra shift to higher energy.

Using a 1st-moment analysis, the position of the main Kβ$_{1,3}$ peak has been calculated for each S-state. Based on the shifts, or lack thereof, of the 1st moments (<E>), it was concluded that Mn is oxidized during the S$_0$ to S$_1$ and S$_1$ to S$_2$ but not oxidized during the S$_2$ to S$_3$ transition. The results (shown as difference spectra in Fig. 2, *Right*) show a shift in energy between the S$_0$ and S$_1$ state spectra and between the S$_1$ and S$_2$ state spectra and seen in the derivative-shaped difference spectra. However, there is very little change between the S$_2$ and S$_3$ states, as seen in the difference spectrum (Messinger et al., 2001).

C. Oxidation State Changes During S-State Transitions

Besides determining whether Mn is oxidized or not during the S-state transitions, both XANES and XES also allow one to assign the oxidation states of the Mn atoms. This is often done by comparison to Mn model compounds.

1. S$_1$ to S$_2$ Transition

Mn K-edge XANES spectra (Fig. 1, *Middle* and *Right*) and the Kβ$_{1,3}$ emission spectra (Fig. 2, *Right*) indicate the presence of Mn oxidation from Mn$_4$(III$_2$,IV$_2$) to Mn$_4$(III,IV$_3$) during the S$_1$ to S$_2$ transition (Roelofs et al., 1996; Messinger et al., 2001), where the S$_2$ state is characterized by the multiline (MLS) or the g=4.1 EPR signal (Cole et al., 1987). This conclusion is corroborated by several other spectroscopic studies (Saygin and Witt, 1987; Kretschmann et al., 1988; Styring and Rutherford, 1988; Evelo et al., 1989; Dekker, 1992; Sharp, 1992) and is also confirmed by EPR spectroscopic measurements. S$_2$-state EPR multiline signal simulations (Hasegawa et al., 1998; Hasegawa et al., 1999) and ^{55}Mn ENDOR spectroscopy on the S$_2$ state (Peloquin et al., 2000) are most consistent with the oxidation states of Mn$_4$(III,IV$_3$); however, other simulations (Zheng and Dismukes, 1996) prefer oxidation states of Mn$_4$(III$_3$,IV) in the S$_2$ state.

If the S$_2$ state is proposed to be either in the

$Mn_4(III,IV_3)$ or the $Mn_4(III_3,IV)$ oxidation states, then the oxidation states of Mn in the S_1 state must be either $Mn_4(III_2,IV_2)$ or $Mn_4(III_4)$, which are both one-electron reductions from the oxidation-state proposals for the S_2 state. Although the oxidation state of $Mn_4(III_4)$ for the S_1 state has been suggested by a few groups (Zheng and Dismukes, 1996; Kuzek and Pace, 2001; Chapter 12, Ahrling et al.), the XANES spectrum or its 2nd derivative of the S_1 state (Figs. 1 *Middle* and *Right*) shows that its edge shape is unlike the edge shape observed for Mn(III) complexes. When the XANES spectrum of the S_1 state, or its 2nd-derivative, is fit using Mn(III) and Mn(IV) model compounds, it cannot be fit well using only Mn(III) model compounds (Riggs et al., 1992; Yachandra et al., 1993). Furthermore, inspection of the only available set of tetranuclear Mn complexes with all O ligation, four distorted $Mn_4(III_3,IV)$ cubanes, shows XANES inflection point energy (IPE) values at ~6551 eV for these complexes (Cinco et al., 1999) consistent with the S_0-state XANES IPE of 6550.8 eV and lower than the S_1-state XANES IPE of 6552.9 eV. These results are consistent with the conclusion that the oxidation states of Mn in the S_1 state are $Mn_4(III_2,IV_2)$, not $Mn_4(III_4)$.

An oxidation-state assignment of $Mn_4(III_2,IV_2)$ is also consistent with recent Kβ XES experiments on the S_1 state. In fitting the $K\beta_{1,3}$ emission spectrum for the S_1 state, Bergmann et al. (1998) found that the best fit to the experimental data was obtained using equal amounts of the $K\beta_{1,3}$ emission spectra from Mn(III) and Mn(IV) model compounds; the fit was significantly worse if only Mn(III) or only Mn(IV) was used for the fit (Bergmann et al., 1998). It is therefore most likely that the oxidation states for Mn are $Mn_4(III_2,IV_2)$ in the S_1 state and $Mn_4(III,IV_3)$ in the S_2 state.

2. S_0 to S_1 *Transition*

The Mn K-edge XANES spectra for the S_0 to S_1 transition, displayed in Fig. 1, *Middle*, and the 2nd derivatives (Fig. 1, *Right*) show a clear shift of 2.1 eV (as determined by the 2nd-derivative IPE values) in the XANES edge position. In addition, the S_1/S_0 Kβ XES difference spectrum, shown in Fig. 2, *Right*, is derivative-shaped, which is indicative of Mn oxidation during this transition. Because the S_1 state has Mn oxidation states of $Mn_4(III_2,IV_2)$, as detailed above, the changes in the X-ray spectroscopic data could be due to either a Mn(II) to Mn(III) oxidation or a Mn(III) to Mn(IV) oxidation.

The finding that the S_1-S_0 XANES difference spectrum (Fig. 1, *Middle*) is somewhat different from the S_2-S_1 difference spectrum suggests that the S_0 to S_1 transition most likely reflects a Mn(II) to Mn(III) oxidation. The shape of the XANES edge is different for the S_0-state and S_1-state spectra; this is shown in part by the peak at 6548 eV in the 2nd derivative of the S_0-state XANES spectrum (Fig. 1, *Right*). This is suggestive of the presence of Mn(II), based on comparison to the 2nd derivatives of Mn(II)-containing model compounds. The significantly larger shift in the 2nd-derivative IPE values for the S_0 to S_1 transition compared to the S_1 to S_2 transition is also indicative for a Mn(II) to Mn(III) oxidation. This is based on the finding that, for homologous sets of model compounds, the shifts in the IPE value for Mn(II) to Mn(III) oxidations are usually larger than those seen for Mn(III) to Mn(IV) oxidations.

Other spectroscopic studies (Saygin and Witt, 1987; Kretschmann et al., 1988; Styring and Rutherford, 1988; Evelo et al., 1989; Guiles et al., 1990a; Dekker, 1992; Sharp, 1992; Messinger et al., 1997a,b; Åhrling et al., 1998) concur that Mn oxidation occurs during the S_0 to S_1 transition. The greater spectral width of the S_0-state EPR multiline signal compared to the S_2-state EPR multiline signal has been attributed to the presence of Mn(II) in the S_0 state (Messinger et al., 1997a,b; Åhrling et al., 1998), which suggests a Mn(II) to Mn(III) oxidation for the S_0 to S_1 transition. The presence of Mn(II) in the S_0 state may also explain why Y_D^{ox} can oxidize the S_0 state to the S_1 state, but not the S_1 state to the S_2 state.

The Kβ XES and XANES difference spectra, in addition to other spectroscopic data are consistent with the assignment of the S_0 to S_1 transition as a Mn(II) to Mn(III) oxidation. Therefore, the oxidation states of Mn in the S_0 state are proposed to be $Mn_4(II,III,IV_2)$, which change upon Mn oxidation to $Mn_4(III_2,IV_2)$ in the S_1 state, although the oxidation states of $Mn_4(III_3,IV)$ for the S_0 state cannot be unequivocally excluded.

3. S_2 to S_3 *Transition*

The most controversial S-state transition has been the S_2 to S_3 transition. Most debate has focused on whether this transition is a Mn-centered (Ono et al., 1992; Iuzzolino et al., 1998) or ligand-centered (Guiles et al., 1990b; Roelofs et al., 1996; Messinger et al., 2001) oxidation. In addition, a redox isomerism between Mn and ligands has been proposed for the S_3 state (Renger, 1997). If Mn were to be oxidized during the S_2 to S_3 transition, the oxidation would have to be a Mn(III) to Mn(IV) transition. A Mn(IV) to Mn(V) transition is unlikely to occur with Mn(III) still present in the complex given the proposed reactivity of the Mn(V) ion. Moreover, Mn(V) has a very distinctive Mn XANES spectrum that has not been observed in PS II preparations (V. Yachandra, unpublished). Thus, it would be expected that the XANES and Kβ XES difference spectra, as well as the observed shifts in the XANES IPE values and the Kβ emission spectra 1st-moment values, <E>, would be essentially identical to the S_1 to S_2 transition, where a Mn(III) to Mn(IV) oxidation also occurs. However, as described below, the spectroscopic results for the S_2 to S_3 transition are completely different from those of the S_1 to S_2 transition.

The XANES results from Fig. 1 provide strong support for a ligand-based oxidation of the OEC occurring during the S_2 to S_3 transition, based on the small (0.3 eV) shift in the XANES 2nd-derivative IPE values. The fact that the S_3-S_2 XANES difference spectrum is significantly different from the S_2-S_1 difference spectrum (Fig. 1, *Middle*) is inconsistent with a Mn(III) to Mn(IV) oxidation occurring during the S_2 to S_3 transition. Instead, the S_3-S_2 XANES difference spectrum shows how the shape of the XANES edge changes between the S_2 and S_3 states, which is consistent with a ligand-based oxidation.

Therefore, based on the XANES data, it is reasonable to suggest that, a ligand radical is formed in the S_3 state in lieu of Mn oxidation; this will be denoted by $Mn_4(III,IV_3)^{\bullet}$. This interpretation is reinforced by the Kβ emission spectra and especially, the Kβ XES difference spectra from Fig. 2, *Right*. The difference spectra show that the derivative-shaped difference spectrum that is expected if Mn is oxidized, as in the S_0 to S_1 and S_1 to S_2 transitions, is absent in the S_2 to S_3 transition. In addition, the <E> value of 6490.157 eV for the S_3 state argues against Mn oxidation during the S_2 to S_3 transition, because it is inconsistent with a $Mn_4(IV_4)$ oxidation state, which is required for the S_3 state if Mn is oxidized during the S_2 to S_3 transition. Comparison of the S_3-state <E> value to the <E> values from 18 different monomeric, dimeric, trimeric, and tetrameric Mn(IV) model compounds with different ligands, including Cl^-, shows that the S_3-state <E> value is higher than the <E> value for any of the Mn(IV) compounds studied. It is difficult to explain this result unless Mn(III) is still present in the S_3 state, which means that, based on the $Mn_4(III,IV_3)$ redox states derived for the S_2 state, a Mn-based oxidation cannot occur during the S_2 to S_3 transition. The EXAFS studies from the S_2 state described below also support this assignment.

D. Summary of Oxidation State Assignments

The Mn K-edge energy and shape do not depend solely on the oxidation state of the Mn atoms, but also on the ligand environment. This is caused by mixing of the ligand and the Mn atomic orbitals. It is possible that a change in structure and ligand environment will influence the main-edge energy and shape. Therefore, care must be exercised when correlating the Mn K-edge energies to Mn oxidation states without taking into account the nature of the ligand environment. This is especially a problem when sets of compounds with different ligand structures, different nuclearities, and different analysis methods to determine edge positions are used to infer oxidation-state information about biological systems, such as in Kuzek and Pace (2001) and Carrell et al. (2002). However, numerous studies have shown that there is a clear correlation between Mn oxidation state and Mn K-edge energy if the ligand environment stays the same, i.e. the IPE shifts to a higher energy upon oxidation within sets of homologous compounds.

A detailed XANES and XES study by Visser et al. (2001) of homologous di-μ-oxo and mono-μ-oxo bridged binuclear compounds in different oxidation states shows that in contrast to Mn K-edge XANES, Kβ XES spectra show much less dependence on ligand environment. The shifts in XES spectra are the same for a Mn(III) to Mn(IV) oxidation, irrespective of whether the Mn is part of a di- or mono-μ-oxo bridged structure (Visser et al., 2001). We have also completed a XES study of homologous sets of tri- and tetranuclear Mn compounds in different oxidation states and we have found that the XES spectra are much less dependent on the ligation or structure and are primarily dependent on the oxidation state of Mn (V. Yachandra, unpublished).

Considering both the limitations and strengths of the two methods of XANES and XES, by comparison with numerous Mn models and the knowledge from EXAFS data (see below), we have proposed the oxidation states shown in Fig. 3. Figure 3 summarizes the Kβ XES and XANES flash patterns from our most recent and in our opinion the most comprehensive study that leads to the conclusions about Mn oxidation

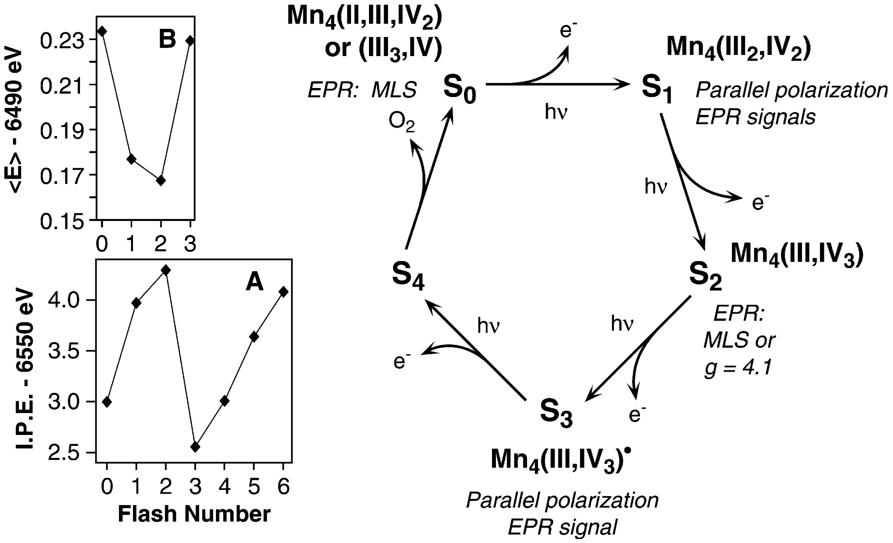

Fig. 3. Left. (A) Inflection-point energy (IPE) in eV of the Mn K-edge of PS II membranes as a function of the number of applied flashes. (B) The first moments of the Mn Kβ emission spectra (<E>) as a function of flash number. The Mn K-edge shifts to higher energy as Mn is oxidized. The first moment of the Mn Kβ fluorescence shifts to lower energy as Mn is oxidized. The complementary and mutually reinforcing results provide a strong case for Mn oxidation during the S_0 to S_1 and S_1 to S_2 advances but no Mn-centered oxidation at the S_2 to S_3 advance. *Right.* The S-state scheme for O_2 evolution and the oxidation states that are consistent with the EPR signals and the X-ray absorption and emission spectroscopy results. Adapted from Messinger et al. (2001).

states. Both spectroscopies show a clear shift in the spectra to higher energy for XANES spectroscopy and lower energy for Kβ XES between the samples given 0 and 1 flashes indicating the presence of Mn oxidation during the S_1 to S_2 transition. The small change between samples given 1 and 2 flashes in both spectroscopies provides strong support for the S_2 to S_3 transition proceeding without a Mn-based oxidation. On the next transition, $S_3 \rightarrow [S_4] \rightarrow S_0$, O_2 is released, shifting the position of the spectra of samples given 3 flashes to lower energy for XANES spectroscopy and higher energy for Kβ XES. These flash patterns are explained by the proposed oxidation states of the Mn cluster in the S_0, S_1, S_2, and S_3 states, as shown. These oxidation states are: S_0: $Mn_4(II,III,IV_2)$ or $Mn_4(III_3,IV)$, S_1: $Mn_4(III_2,IV_2)$, S_2: $Mn_4(III,IV_3)$, S_3: $Mn_4(III,IV_3)^{\bullet}$, where the superscript dot represents an oxidation that is not Mn centered.

III. Structure of the Manganese Cluster

Extended X-ray absorption fine structure (EXAFS) spectra at the Mn K-edge results from the modulation of the absorption cross section by the constructive and destructive interference of the 1s photoelectron wave with that backscattered from neighboring atoms (Sayers et al., 1971). The EXAFS modulations can be theoretically modeled to derive exquisitely detailed information about the distance from Mn to neighboring atoms to ~4 Å, often to an accuracy as precise as 0.015 Å (Yachandra, 1995). However, determination of the number of such interactions is susceptible to many uncertainties and can often be as large as 25%. The EXAFS approach has been used to determine the distances from Mn and identify the backscattering atoms of the Mn cluster present in the OEC. It is not possible to distinguish between O or N. But it is often facile to distinguish between light atoms such as N, or O, which are potential ligand atoms and backscattering from a heavier atom such as Mn or Ca that would only be present in a multi- or hetero-nuclear Mn complex. To interpret the results in terms of the coordination environment of the Mn, it has been necessary to examine a number of inorganic complexes of known structure, generously provided to us by our collaborators (Guiles et al., 1990a; DeRose et al., 1994; Cinco et al., 1999). The EXAFS spectrum is usually presented as a Fourier transform (FT), which is similar to a radial distribution function with each Fourier peak representing shells of neighboring atoms from the absorbing atom. Dichroism resulting from oriented membranes can be used to derive information about the vectorial direction of the particular interaction. A typical Fourier transform from an S_1 state is shown in Fig. 4, *Top* (Yachandra et al., 1993; DeRose et al., 1994) and from oriented PS II membranes in the S_1 state in Fig 4, *Bottom* (Mukerji et al., 1994). Three distinct Fourier peaks are resolved in Fig. 4, *Top*, and dichroism is evident in all of the peaks in Fig. 4, *Bottom*.

On the basis of the latest findings, we conclude that each Mn is surrounded by a first coordination shell of O or N atoms at ~1.8 to ~2.1 Å (Fourier peak I), a set of Mn atoms at ~2.7 Å (Fourier peak II) and additional Mn and Ca at ~3.3 Å (Fourier peak III). Using model-compound data, it was straightforward to assign the two or three 2.7 to 2.8 Å Mn-Mn vectors to di-μ-oxo or hydroxo bridges between pairs of Mn atoms and the 3.3 Å Mn-Mn vector to one or two mono-μ-oxo bridged or similar longer interactions (Kirby et al., 1981; Yachandra et al., 1986, 1987; McDermott et al., 1988; George et al., 1989; Penner-Hahn et al., 1990; MacLachlan et al., 1992; DeRose et al., 1994; Mukerji et al., 1994; Kusunoki et al., 1995; Robblee et al., 2001). Furthermore, studies using Sr to replace Ca and, subsequently, direct measurements using Ca EXAFS, show unambiguously the presence of one or two 3.4 Å Mn-Ca vectors where the bridging motif could also be mono-μ-carboxylato or mono-μ-hydroxo (see below). The use of vector terminology to describe these interatomic interactions is particularly appropriate because of the direction information available from dichroism measurements on oriented samples. Furthermore, analysis of the EXAFS leads to the conclusion that the di- or mono-μ-oxo bridged Mn and Ca vectors are not co-linear; that is any three metal atoms in the cluster cannot be linear.

On the basis of such data many topological tetranuclear Mn structures (**A** through **K**) compatible with the observed EXAFS data have been presented (DeRose et al., 1994) (Fig. 5). These models have been described in detail (DeRose et al., 1994; Robblee et al., 2001). However, until recently only one of those options, **A**, was widely used as a working model, although options **E**, **F** and **G** (the nomenclature was initially introduced in DeRose et al. (1994)) have been shown to be preferred on the basis of EPR and ENDOR simulations (Hasegawa et al., 1999; Peloquin and Britt, 2001). Some of the structures, **A** through **K**, are less likely. Structure **C** and variations consisting of two isolated di-μ-oxo Mn–Mn moieties are preferred by Pace and co-workers based on their EPR simulations (Smith and Pace, 1996) but **C** is not widely accepted on the basis of EPR simulations by other groups (Boussac and Rutherford, 2000; Britt et al., 2000; Peloquin et al., 2000) or EXAFS data (Latimer et al., 1998). It is also physically impossible

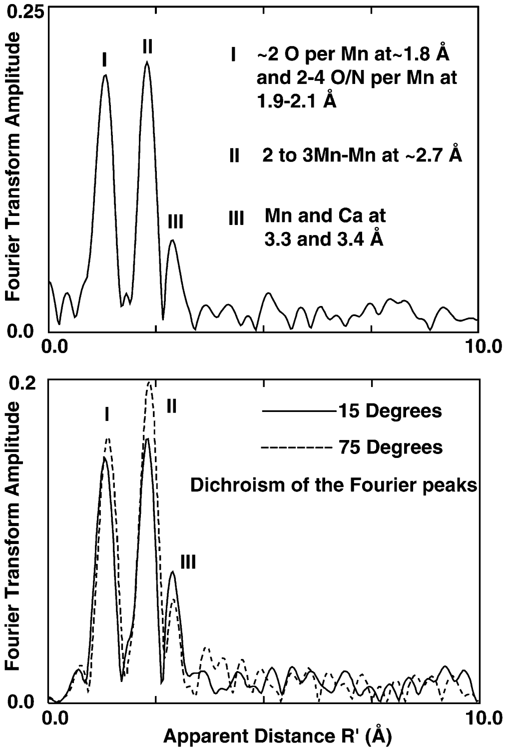

Fig. 4. Typical Fourier transform of the EXAFS spectrum from a S_1 state sample from an isotropic sample (*Top*) and oriented sample (*Bottom*). The three main Fourier peaks labeled I, II and III are assigned to ~ 2 O ligand atoms per Mn at 1.8 Å and 2-4 N/O ligand atoms per Mn at 1.9–2.1 Å (Fourier peak I), 2-3 Mn-Mn interactions at ~2.7 Å (Fourier peak II), and Mn and Ca at 3.3 and 3.4 Å (Fourier peak III), respectively. The dichroism of the Fourier peaks I, II and III is clear and can be used to determine the orientation of the vectors in the PS II membrane. Fourier peak II, that has been assigned to Mn-Mn interactions at ~2.7 Å, is maximal when the e-vector of the X-rays is parallel to the membrane plane (the angle on the figure is between the membrane normal and the X-ray e-vector.). Adapted from Yachandra et al. (1993), DeRose et al. (1994) and Mukerji et al. (1994).

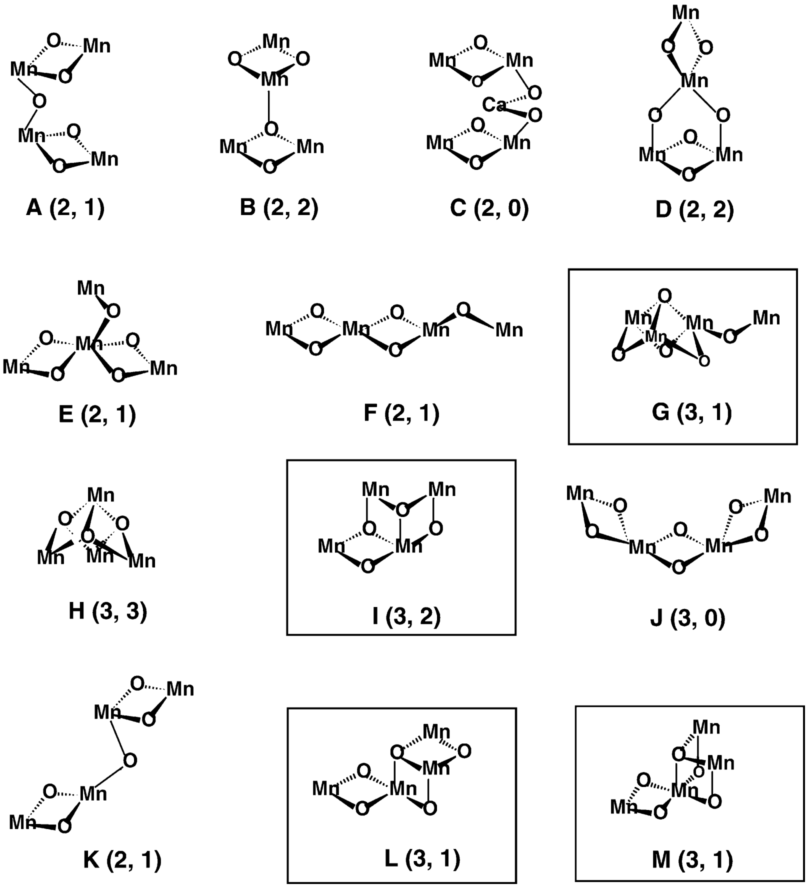

A (2, 1) B (2, 2) C (2, 0) D (2, 2)

E (2, 1) F (2, 1) G (3, 1)

H (3, 3) I (3, 2) J (3, 0)

K (2, 1) L (3, 1) M (3, 1)

Fig. 5. Topological models for the Mn complex identified as compatible with the EXAFS data by DeRose et al. (1994) and Robblee at al. (2002). The numbers in parenthesis are the number of short 2.7 to 2.8 Å Mn-Mn vectors and long 3.3 to 3.4 Å Mn-Mn vectors. The options **G**, **I**, **L** and **M** all have 3 short 2.7 to 2.8 Å Mn-Mn vectors and are in better agreement with the X-ray diffraction studies; options **E**, **F** and **G** have been identified as compatible with EPR and ENDOR data. Option **G** or a topological isomer seems to be the best model by all presently available criteria; X-ray diffraction, EXAFS and EPR.

with four Mn atoms to obtain three Mn–Mn distances (see below) at 2.7 – 2.85 Å with two separated di-μ-oxo Mn–Mn moieties. Structure **H**, with three 3.3 Å Mn–Mn distances is unlikely, as shown by the EXAFS spectra from a similar set of complexes – a series of distorted cubanes (Cinco et al., 1999). The more likely candidates were considered to be **A**, **E**, **F**, **G** or **K** on the basis of EXAFS and EPR data; only **G** contained three Mn-Mn distances at ~2.7 Å, while the others had two such interactions.

A. Heterogeneity in the Mn-Mn Distances and Structural Implications

As mentioned above determining the number of Mn-backscattering atoms can be difficult. The number of the Mn-Mn 2.7 and 3.3 Å vectors (shown in parenthesis in Fig. 5) are especially important in this endeavor as these data directly lead or preclude certain arrangements of the Mn atoms that comprise the Mn cluster. The distance of the Mn-Mn vectors (at ~2.7 and 3.3 Å) is particularly important because it is easily the most reliably determinable parameter from the Mn EXAFS spectra of PS II. It is informative to focus on

Table 1. Curve-fitting results for Fourier peak at ~2.7 Å that is characteristic of oxo-bridged Mn moieties from the S-states

S-state	References	R_1 (Å)	R_2 (Å)	N_1	N_2	N_1:N_2
S_0^* state	Table III from Guiles et al. (1990a)	2.69	2.87	1.0	0.5	2:1
S_2 (g = 4.1) state	Table 4B from Liang et al. (1994)	2.72	2.85	0.76	0.44	1.7:1
NH_3-inhibited S_2 state	Table 1 from Dau et al. (1995)	2.71	2.86	0.75	0.5	1.5:1
F^--inhibited S_2 state	Table 2 from DeRose et al. (1995)	2.71	2.85	0.8	0.4	2:1
S_3 state	Table 1B from Liang et al. (2000)	2.82	2.95	0.7	0.4	1.8:1
S_0 state	Table 3 from Robblee et al. (2002)	2.72	2.86	1.05	0.46	2.3:1
S_0 state	Table 4 from Robblee et al. (2002)	2.72	2.85	1.02	0.51	2:1

N_1 and N_2 are the number of Mn-Mn interactions, normalized to one Mn in the Mn_4 complex, at the two distances R_1 and R_2, respectively. An N of 1 translates to two Mn-Mn distances and a N of 0.5 translates to 1 Mn-Mn distance at the corresponding distance. The N_1:N_2 ratio of 2:1 in the ~2.7 and ~2.8 Å Mn-Mn distances shows there are a total of 3 such short Mn-Mn distances in the OEC.

the ~2.7 Å Mn-Mn distance. When only one Mn-Mn 2.7 Å distance can be derived from the data as in the case of the S_1 and S_2 states, then one is constrained by the uncertainty in the number of such interactions that is inherent to the EXAFS methodology; it is at present two or three such Mn-Mn interactions. However, when the distance degeneracy is lifted and there are two resolvable 2.7 or 2.8 Å Mn-Mn distances then one can determine the number of such vectors to a much higher accuracy because one can only have an integral number of each of such interactions.

Interestingly, when we examined states that exhibited such heterogeneity in the 2.7 Å Mn-Mn distances, it became quite clear that there was distinct preference for the existence of three such Mn-Mn vectors as described below (summarized in Table 1). Figure 6, *Left* shows the Fourier transforms (FT) of the k^3-weighted EXAFS data from the S_0 and S_1 states. The Fourier peak II was isolated and fit to the EXAFS equation with one or two distances for the S_0 and S_1 states. Figure 6, *Right* shows the best fits to two Mn-Mn distances for the S_0 state as a function of the number of each of the Mn-Mn interactions. The contour plot graphically illustrates that the global minimum at two Mn-Mn interactions at ~2.7 Å and one Mn-Mn interaction at ~2.85 Å is very well defined (Robblee et al., 2002).

We have re-examined the data from the S_0* (S_0 state induced by NH_2OH incubation), the g=4.1 S_2, the NH_3- or F^-inhibited S_2, and the S_3 states, where we have shown that there is distance heterogeneity in the Mn-Mn vectors. The results of this re-examination are given in Table 1, which show that none of the S-states that exhibit distance heterogeneity are best fit by an equal N value for both Mn–Mn shells; the fit results from these S-states are in fact more consistent with a 2:1 N_1:N_2 ratio, where N_1 corresponds to the shorter distance. In each case, the ratio of the number of the two Mn-Mn interactions was ~2:1. This leads us to think that there may be three Mn interactions at ~2.7 Å in the Mn cluster in its native state, one of which is perturbed in the S_0, F^-- and NH_3-inhibited S_2 and the g=4.1 S_2 states, and all three are perturbed in the S_3 state.

On the basis of these re-evaluations of the results from the S_0 state and earlier data, it is important to consider the options that include three di-μ-oxo bridged moieties in the Mn cluster. Figure 5 shows several such options, **G**, **I**, and **J**, that were proposed earlier, and two newer options, **L** and **M**, among several others that can be conceived. Options **J** and **I** are less likely structures because **J** lacks a Mn-Mn interaction at 3.3 Å, and **I** has two such interactions. The EXAFS data from an inorganic compound (Auger et al., 1990) with the motif in option **J** is very different from that obtained from a PS II sample (V. Yachandra, unpublished). Options **G**, **L** and **M** all have three di-μ-oxo bridges and one mono-μ-oxo bridge; that is three 2.7 Å and one 3.3 Å Mn-Mn interactions. Options **L** and **M** are also similar to the structure proposed on the basis of density functional theory calculations although Ca is not included in **L**

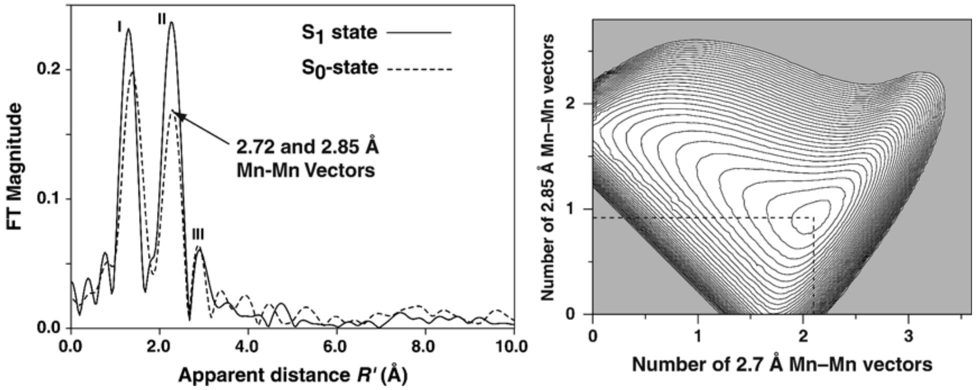

Fig. 6. Left. Fourier transforms of the S_0 (dashed line) and S_1 state (solid line) of the Mn-EXAFS spectra. The main Fourier peaks are labeled I, II and III. There are clear differences in amplitude and position of these peaks between the S_0 and S_1 states. The peak labeled II is from Mn-Mn interactions at ~2.7 Å, and in the S_0 state this vector is best fit to two distances at 2.72 and 2.85 Å. *Right.* The contour plot shows the fit-quality-parameter ε^2 for the S_0 state plotted versus the number of the two Mn-Mn interactions. The dashed lines shows the distinct minimum at one Mn-Mn vector at 2.85 Å and two Mn-Mn vectors at 2.7 Å. Adapted from (Robblee et al., 2002).

and **M** and is an integral part of the Siegbahn model (Siegbahn, 2000).

In addition to the constraints imposed by considering the EXAFS and EPR data, a preliminary structure of the OEC has been recently reported based on X-ray crystallographic data from PS II (Zouni et al., 2001; Kamiya and Shen, 2003; Ferreira et al., 2004; Chapters 19–21) and a further criterion for narrowing the choice of favored cluster geometries comes from these X-ray crystallography data of PS II. These data are most consistent with an OEC that is asymmetric and shaped somewhat like a 'Y'. The arrangement of the Mn atoms has been described as pear-shaped (an elongated ellipsoid) with all four Mn lying approximately in the same plane. Presently, **G**, **L** and **M** are qualitatively in agreement with the asymmetry seen in the electron density of the Mn cluster (Zouni et al., 2001) and should be considered as possibilities for a topological model of the OEC based on the insights developed from the EXAFS spectroscopy results, with option **G** being the best in terms of being compatible with the most criteria; electron density, EPR, and EXAFS. However, as confirmed by Mn and Sr EXAFS studies (Latimer et al., 1995; Cinco et al., 1998) the OEC is most accurately described as a Mn/Ca heteronuclear cluster; therefore, Ca should be incorporated into each of the proposed structures so that 1–2 Mn–Ca vectors exist which are oriented close to the membrane normal (Ferreira et al., 2004; Chapter 21).

B. S-State Transitions and Structural Changes

Although EXAFS studies may not be able to uniquely identify the structure of the Mn complex, they are invaluable in understanding the changes in structure, if any, that might be occurring during the S-state transitions. As noted above, EXAFS is exquisitely sensitive to distances of neighboring atoms from Mn and hence can provide an unique window into how the Mn cluster changes as it proceeds through the catalytic cycle, as summarized in Fig. 7. These changes in structure provide a rationale for testing various mechanisms that have been proposed as described below.

1. S_1 to S_2 (MLS) Transition

EXAFS studies of the S_1 state and the S_2 state characterized by the multiline EPR signal revealed that the Mn–Mn distances are essentially the same: ~2.7 Å and 3.3 Å in both states. This distance is consistent with those found in numerous studies of di- and mono-μ-oxo-bridged and Mn_2(III,IV) and Mn_2(IV,IV) complexes. Oxidation of a mono- or di-μ-oxo bridged Mn motif from (III,III) to (III,IV) or from (III,IV) to (IV,IV) has minimal effect on the Mn-Mn separation in many inorganic models (Wieghardt, 1989; Pecoraro, 1992; Pecoraro and Hsieh, 2000).

Interestingly, EXAFS studies on oriented PS II in the S_1 and S_2 states show that there maybe heterogeneity in the 2.7 Å vector, a contention that is supported

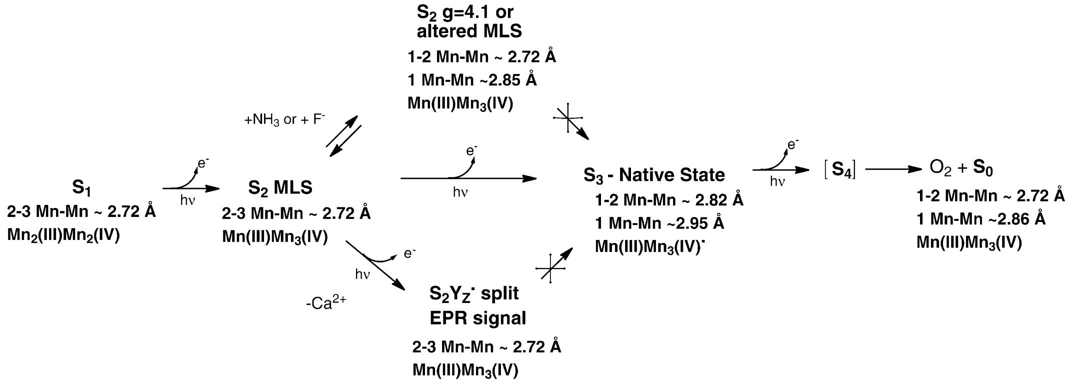

Fig. 7. Summary of the changes in oxidation states and Mn–Mn distances at 2.7 to 3.0 Å in the native S_1, native S_2, modified S_2, S_3' ($S_2Y_Z^{\bullet}$), native S_3 and S_0 states of PS II as determined by Mn EXAFS.

by related studies on modified S_2 states. This Mn-Mn vector has been determined to be at an average angle of ~60° to the membrane normal (Mukerji et al., 1994; Dau et al., 1995).

2. S_1 to S_2 (g=4.1) Transition

The inequivalence of the di-μ-oxo bridged Mn units becomes more evident in the S_2 state that is prepared by illumination at 130 K and characterized by the *g*=4.1 EPR signal (Liang et al., 1994). Similar results were obtained with NH_3-treated and annealed S_2 state samples (Dau et al., 1995) and in F^--treated samples (DeRose et al., 1995). The scheme in Fig. 7 shows that there are paths from the MLS S_2 state that lead to two states: the S_2-*g*=4.1 state inhibited by NH_3/F^- or the $S_2Y_Z^{\bullet}$ states; neither of these states can proceed to the physiologically relevant S_3 state. These states are depicted in Fig. 7 as branching away from the normal pathway leading to the S_3 state by photon absorption. However, the S_2-*g*=4.1 state generated by 820 nm illumination at 130 K (Boussac et al., 1996) can proceed to an S_3 state (Zimmermann and Rutherford, 1986). In the modified S_2 states, one of the Mn-Mn distances increases to ~2.85 Å, whereas there is very little change in the other one or two 2.7 Å or the 3.3 Å Mn-Mn distance. With the degeneracy of the 2.7 Å lifted, it has been possible by studying the dichroism of the Fourier peak, to assign the relative orientation of the 2.7 and 2.85 Å vectors (Dau et al., 1995), which are oriented at 55° and 67° respectively to the membrane normal.

The NH_3-treated and F^--treated samples cannot advance beyond the modified S_2 state ($S_2Y_Z^{\bullet}$ state). It is likely that F^- or NH_3 prevent the oxidation of a ligand atom, thereby blocking structural changes from occurring that are necessary for the formation of the S_3 state, and thus inhibiting O_2 evolution activity. In the case of NH_3, it is probably due to an amido-group (NH_2^-) replacement of the oxo-bridge involved in oxidation. The modification of the MLS spectra upon addition of NH_3 (Beck et al., 1986) and ESEEM studies using $^{14}NH_3$ and $^{15}NH_3$ demonstrated that NH_3 becomes a ligand of Mn (Britt et al., 1989). The asymmetry parameter derived from ESEEM results suggested that the amido group is likely to be a bridging ligand (Britt et al., 1989). It is probable that the oxo-bridge that is displaced by NH_3 is oxidized during the S_2 to S_3 transition (see next section).

3. S_2 to S_3 Transition

Earlier XAS data from the S_3 state samples produced by a cryogenic double-turnover method indicated increased disorder in the peak at 2.7 Å; that a structural change that involved the lengthening of the Mn-Mn distance was occurring between the S_2 and S_3 states and was absent during the S_1 to S_2 state transition (Guiles et al., 1990b). More recent detailed analysis of data from native S_3 state samples created under physiological conditions with saturating actinic flash illumination show there is a significant change in the 2.7 Å Mn-Mn distances that characterize the di-μ-oxo bridged Mn-Mn; with an increase in the short Mn-Mn distances from 2.7 Å to ~2.8 and ~3.0 Å (Liang et al., 2000).

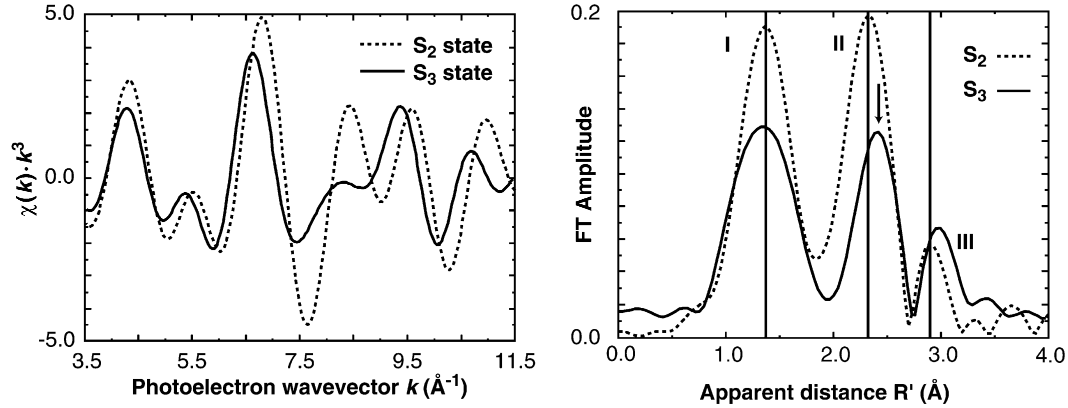

Fig. 8. Left. Fourier-filtered *k*-space EXAFS data from S_2 (dashed line) and S_3 (solid line) state of PS II samples. The differences in phase, frequency and amplitudes between the raw S_2 and S_3 state EXAFS spectra are very obvious in these spectra. *Right.* Fourier transform power spectra of S_2 (dashed line) and S_3 (solid line) states of PS II. The major Fourier peaks are labeled I, II and III. The spectra are clearly different between the S_2 and S_3 states. There is a reduction in amplitude in all three peaks in the S_3 state compared to the S_2 state. More importantly, peaks II and III are at a greater apparent distance R' for the S_3 state compared to the S_2 state as shown.

The perturbation in the Mn-Mn distances is different from that observed in the modified S_2 states. Each of the altered S_2 states gives a fit that is consistent with the alteration of one of the Mn-Mn distances from ~2.72 to 2.85 Å. Unlike the modified S_2 states, the position of Fourier peak II from the native S_3 state clearly shifts to a longer distance in the FTs (Fig. 8) with one or two Mn-Mn distances of 2.82 Å and one Mn-Mn distance of 2.95 Å (Liang et al., 2000). These results underscore the point that during the S_2 to S_3 transition under physiological conditions, *all* of the di-μ-oxo-bridged Mn-Mn units undergo structural changes that lead to an increase in the Mn-Mn distances. A change in the Mn-Mn distance from 2.7 to 3.0 Å was also observed in samples that had been depleted of Ca by NaCl treatment (MacLachlan et al., 1994). The best fits for the Mn-O/N shell shorter Mn-O distance is characteristic of Mn-O bridging distances and it increases from 1.80 Å in the S_2 state to 1.86 Å in the S_3 state. This is a significant change, and it provides additional evidence for the involvement of the bridging oxygen atoms during the S_2 to S_3 transition.

The results from isotropic S_3 samples are supported by polarized EXAFS studies on oriented PS II in the native S_3 state. The data confirm that the two Mn-Mn vectors units are not equivalent. The polarized EXAFS data are different from those observed in the S_2 state (Mukerji et al., 1994; Dau et al., 1995). Fourier peak II of S_3 is dichroic and is readily resolved to Mn-Mn distances of ~2.8 Å and ~3.0 Å, each with its own distinct projection on the membrane normal (Fernandez et al., 1998). Schiller et al. (1998) have reported results on the oriented S_3 state, showing an increase in the amplitude of Fourier peak II that is interpreted as an increase in the number of 2.7 Å Mn-Mn interactions in the S_3 state. However, a closer examination of their FTs indicates that Fourier peak II occurs at a longer distance and is broader compared to that in the S_2 state.

In the S_3 state it is seen that Fourier peak III at ~3.3 Å occurs at a greater apparent distance than that of the S_2 state indicating a lengthening of the two Mn-Mn distances or the Mn-Mn and Mn-Ca distances compared to the S_2 state by 0.04-0.2 Å.

Significant changes are observed in the Mn-Mn distances in the S_3 state compared to the S_1 and the S_2 states (Fig. 8). These changes in Mn-Mn distances are interpreted as consequences of the onset of substrate water oxidation in the S_3 state. Mn-centered oxidation is evident during the S_0 to S_1 and S_1 to S_2 transitions. During the S_2 to S_3 transition, we propose that the changes in Mn-Mn distances are the result of ligand or water oxidation, leading to the formation of an oxyl radical intermediate formed at a bridging or terminal position. The reaction of the oxyl radical with OH^-, H_2O, or an oxo group during the subsequent S-state conversion is proposed to lead to the formation of the O-O bond (Chapter 25).

4. S_2 to S_3' ($S_2Y_Z^{\bullet}$) Transition

The other unproductive state generated from the S_2-MLS state is denoted in Fig. 7 as the S_3' state or $S_2Y_Z^{\bullet}$ state generated in Ca-depleted samples. The Ca-depleted samples are inactive in O_2 evolution, while a broad $g = 2$ EPR signal has been observed in such samples. The $g = 2$ broadened EPR signal has been confirmed to arise from the tyrosine Y_Z radical (Gilchrist et al., 1995; Peloquin et al., 1998) and it is proposed that the signal is broadened by interaction with the spin on the Mn cluster (Lakshmi et al., 1998).

EXAFS analysis from Ca-depleted S_3' state samples ($S_2Y_Z^{\bullet}$) (Latimer et al., 1998) shows that Fourier peak II (Mn-Mn distance of ~2.7 Å) in the FT of S_3' state samples ($S_2Y_Z^{\bullet}$) was invariant relative to that of the native S_2 state sample. The EXAFS fits showed that the ~2.7 Å Mn-Mn distances did not lengthen as observed in the native S_3 state samples and are essentially unchanged from those of the native S_2 state. This finding is surprising because the Mn K-edges from these Ca-depleted samples showed a behavior similar to the native PS II in that little or no shift was observed in the S_2' to S_3' (or $S_2Y_Z^{\bullet}$) transition. This difference between the native S_3 and Ca-depleted S_3' states indicate that the core di-μ-oxo-bridged structure is probably dissimilar in the native S_3 and the S_3' ($S_2Y_Z^{\bullet}$) states, with the structure in the $S_2Y_Z^{\bullet}$ state resembling the native S_2 state structure. It is intriguing how the transfer of one electron from the Mn cluster onto Y_Z result in major changes in the Mn-Mn distances as is observed in the native S_3 state. The roles of the Y_Z and the Mn cluster in the process of water oxidation are clearly delineated by the comparison of the S_3 and the S_3' (or $S_2Y_Z^{\bullet}$) states. Instead of the Mn cluster just providing a scaffolding for water oxidation, this comparison shows that the structural change in the Mn cluster initiated by the transfer of an electron from the Mn cluster to Y_z during the S_2 to S_3 transition might provide the trigger to the chemistry of the formation of the O-O bond, via the formation of a ligand radical. The results show that the Mn cluster is involved in a much more intimate manner in the catalysis than just providing the framework. The implications to the mechanism are significant (Chapter 25).

In Ca-depleted systems the tyrosine Y_Z radical is stabilized and the oxidation of the Mn-OEC and the concomitant changes in Mn-Mn distances are prevented. In the S_3 state, with Ca present, the oxidation equivalent resides on the Mn cluster leading to profound changes in the Mn-Mn distances. Thus, Ca is proposed to play a crucial role in controlling the redox potential and thus the course of the mechanism of water oxidation.

5. S_0 to S_1 Transition

Early EXAFS experiments by Guiles et al. (1990a) with the S_0 state used chemical treatments to get around the problem of low concentrations. However, the S_0 state generated in this manner was designated as S_0^* to emphasize that it is generated through chemical treatment and is thus not a native S-state. Although hampered by a low signal-to-noise ratio and the uncertainty about the relationship between the chemically generated S_0^* state and the native S_0 state, those experiments provided the first evidence from EXAFS that heterogeneity may exist in the 2.7 Å Mn–Mn distances in the S_0 state in the form of a reduced amplitude of Fourier peak II in the S_0^* state relative to that in the S_1 state.

Riggs-Gelasco et al. (1996a) examined reduced S states of the OEC generated by treatment with NH_2OH or hydroquinone and observed a decrease in the amplitude of the 2.7 Å Mn–Mn Fourier peak. This was interpreted as a reduction in the number of Mn–Mn vectors instead of the appearance of distance heterogeneity.

Recent EXAFS experiments by Robblee et al. (2002) show that, in the S_0 state, heterogeneity most likely exists in the 2.7 Å Mn–Mn distances with one or two Mn-Mn distances at 2.72 Å and one Mn-Mn distance at 2.85Å (as described above, see Fig. 6), which can be explained through the protonation of a di-μ-oxo-bridged Mn–Mn moiety and/or the presence of Mn(II) (Chapter 25). The presence of distance heterogeneity in the S_0 state has been exploited in the curve-fitting procedure, whose results are suggestive of the possibility that three di-μ-oxo-bridged Mn–Mn moieties may exist in the OEC instead of the two di-μ-oxo-bridged Mn–Mn moieties that are widely used in proposed structural models for the OEC (see above).

IV. Structural Role of the Calcium Cofactor

Along with Mn and Cl^-, Ca is an essential cofactor in O_2 evolution (Debus, 1992; Chapter 13, van Gorkom and Yocum). Depleting this cofactor suppresses

OEC activity, which can be restored (up to 90%) by replenishing with Ca^{2+}. Partial reactivation (up to 40%) results from addition of Sr^{2+} to Ca-depleted PS II membranes (Ghanotakis et al., 1984; Boussac and Rutherford, 1988b) and no other metal ions can restore activity, making this requirement highly specific for Ca or Sr (Ghanotakis et al., 1985; Ono and Inoue, 1989).

Although Sr^{2+} replenishes the Ca-depleted centers to a similar extent as added Ca^{2+}, the slower kinetics of the OEC turnover yields an overall lower steady-state rate (Boussac and Rutherford, 1988a) (40%) at saturating light intensities. Substitution of Ca with Sr also alters the EPR multiline signal (MLS) from the S_2 state, giving narrower hyperfine splitting and different intensity patterns (Boussac and Rutherford, 1988b; Sivaraja et al., 1989). Most researchers addressing the stoichiometry of the Ca cofactor in PS II now conclude that functional water oxidase activity requires one essential Ca^{2+}, which can be removed by low-pH/citrate or 1.2 M NaCl wash (Cammarata and Cheniae, 1987; Katoh et al., 1987; Ono and Inoue, 1988; Shen et al., 1988; Adelroth et al., 1995). In higher plants, another more tightly bound Ca is associated with the light-harvesting complex (LHC II) and requires harsher treatments for its removal (Han and Katoh, 1993; Chen et al., 1995).

A. Manganese Extended X-Ray Absorption Fine Structure (EXAFS) and Calcium

Several investigations have involved removal of Ca and substitution of various metals into this binding site, followed by EXAFS studies on the Mn cluster. One set of experiments using Mn EXAFS on Sr-reactivated PS II membranes was interpreted to indicate a 3.4–3.5 Å distance between the Ca (Sr) and the Mn cluster (Latimer et al., 1995). This conclusion was based on the observation of increased amplitude in Fourier peak III at 3.3 Å upon replacement of Ca with Sr, a heavier atom and better X-ray scatterer. Analysis of EXAFS spectra from purified PS II membrane preparations indicated a Mn–Ca interaction at slightly longer distance (MacLachlan et al., 1992) (~3.6-3.7 Å). Ca depletion by NaCl-washing of PS II membranes removed the 16 and 23 kDa extrinsic proteins and led to a reduced amplitude for this 3.6 Å feature and because of the lower X-ray scattering ability of Na, this result was interpreted as possible Na^{+} substitution for Ca^{2+} at this distance (MacLachlan et al., 1994). Another Mn EXAFS study (Riggs-Gelasco et al., 1996b) did not detect any changes in the Fourier peak at 3.3 Å when Ca was replaced with Sr^{2+} or Dy^{3+} in PS II reaction center complexes lacking the 16 and 23 kDa extrinsic polypeptides; however, it was proposed that Ca might be linked via a hydrogen bond to the oxo ligand of the Mn cluster.

B. Strontium Extended X-Ray Absorption Fine Structure (EXAFS) and Calcium

1. Isotropic Samples

The most common approach, as described above (Latimer et al., 1995; Riggs-Gelasco et al., 1996b), was to substitute other metals (such as Sr) for Ca and then use Mn EXAFS to detect changes in the cluster. Isolating the Mn-Ca or Sr component of the EXAFS spectrum from the combined EXAFS from all Mn-ligand and Mn-Mn interactions can be difficult. The reverse experiment where one probes for backscattering from Mn using Ca or Sr EXAFS (Ca/Sr cofactor point-of-view for nearby Mn) is an elegant alternative and is more definitive than Mn EXAFS results. Such studies on both isotropic and oriented PS II membranes have yielded unequivocal evidence for the proximity of Ca to the Mn cluster (see below).

Several factors favor Sr as the better cofactor for XAS study. First, the X-ray energies involved (16 keV for the K-edge) are more penetrating and not attenuated by air. The higher X-ray absorption cross-section and fluorescence yield of Sr also make the experiment practicable. The Sr EXAFS-based experiment requires PS II samples with Sr substituted for Ca while maintaining O_2-evolving activity and a stoichiometry of 1 Sr per PS II, to focus on the functional cofactor binding site. Along with reactivated Sr-PS II, an inactivated sample can be prepared by treating with hydroxylamine (NH_2OH) to disrupt the Mn cluster and suppress water oxidase activity (Tamura and Cheniae, 1985).

By using Sr EXAFS on isotropic Sr-reactivated PS II membranes, the proximity of Sr (and implicitly Ca) to within 3.5 Å of the Mn cluster (Cinco et al., 1998) has been confirmed. The finding was based on the presence of a second Fourier peak (peak II, Fig. 9, *Top*) in the Sr EXAFS from functional samples, a peak that is absent from inactive, hydroxylamine-treated PS II. This Fourier peak was found to fit best to two Mn at ~3.5 Å rather than lighter atoms (C, O, P, S, Cl). Both types of samples share similar first coordination shells of oxygen (Peak I, Fig. 9, *Top*).

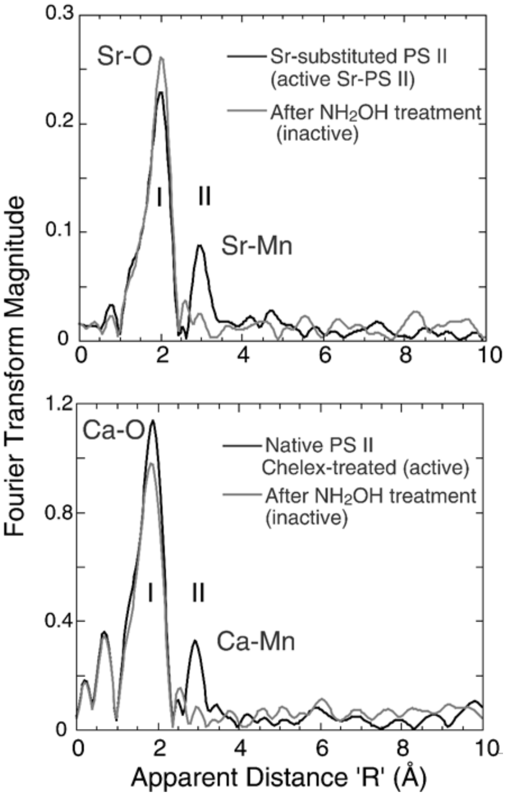

Fig. 9. Top. Fourier transforms of Sr EXAFS for intact and inactive Sr-substituted PS II samples (Chelex-treated). The dominant Fourier Peak I is due to ligating oxygens in the first coordination sphere and is common to both samples. The two Sr-PS II samples differ mainly at the '*R*' = 3.0 Å region, where the intact samples exhibit Fourier Peak II. Disruption of the Mn cluster in NH_2OH-treated sample leads to the absence of Peak II. *Bottom.* Fourier transform of Ca EXAFS from Chelex-treated, layered samples with 2 Ca/PS II with O_2-evolving activity and an S_2 EPR multiline signal. The FTs show the presence of a second Fourier peak in the 2Ca/PS II sample that fits to Ca-Mn that is absent in the control sample where the Mn complex has been disrupted with NH_2OH.

2. Oriented Samples

The technique of using Sr EXAFS has been extended to using polarized Sr EXAFS on layered Sr-substituted samples, to provide important angle information. Polarized EXAFS involves collecting spectra for different incident angles (θ) between the membrane normal of the layered sample and the X-ray electric field vector. Dichroism in the EXAFS can occur, depending on how the particular absorber–backscatterer (A–B) vector is aligned with the electric field. Through analysis of the dichroism, the average orientation (ϕ) of this A–B vector relative to the membrane normal, and the average number of scatterers per absorbing atom (N_{iso}) can be extracted. Constraints on the structural model are then imposed by these parameters.

Sr-substituted PS II samples made by a process of Ca depletion, Sr^{2+} reactivation, and Chelex treatment to remove excess Sr were layered onto flat Mylar films to produce oriented samples (Mukerji et al., 1994; Dau et al., 1995). The Fourier transforms from the polarized Sr EXAFS showed extreme dichroism in Fourier peak II (Fig. 10, *Left*). Nonlinear least-squares regression analysis produced the solid curve shown in Fig. 10, *Right* as the best fit of the 15 data points (angles from six separate samples) and the result translates to 1–2 Sr–Mn vectors with an average angle of 0° or 23° for the average relative angle between the Sr–Mn vectors and the membrane normal depending on the method of analysis.

3. Orientation of the Manganese Complex

The orientation data from the Sr EXAFS experiments can be combined with the dichroism data from Mn EXAFS data to calculate the orientation of the 3.3 Å Mn–Mn vector. The Fourier peak in the Mn EXAFS which contains the Mn–Mn (3.3 Å) and Mn–Ca (3.4 Å) contributions, is dichroic, with an average angle of 43 ± 10° with respect to the membrane normal (Mukerji et al., 1994). By including the Mn-Ca vector at 23°, an angle of ~62° for the 3.3 Å Mn–Mn vector can be calculated. Previous polarized Mn EXAFS experiments on PS II have shown angles of 55° and 67° for the 2.7 Å Mn–Mn vectors (Mukerji et al., 1994; Dau et al., 1995). Thus it follows that all Mn–Mn vectors lie at roughly the same angle (~61°) with respect to the membrane normal, but are not restricted to being collinear, because the PS II membranes are ordered in one dimension only. The electron density from the X-ray diffraction studies (Zouni et al., 2001) are in agreement with such an assignment; the plane containing the Mn electron density is at ~67° to the membrane normal.

C. Calcium Extended X-Ray Absorption Fine Structure (EXAFS)

In a complementary and definitive experiment, Ca K-edge EXAFS studies have been used to probe the

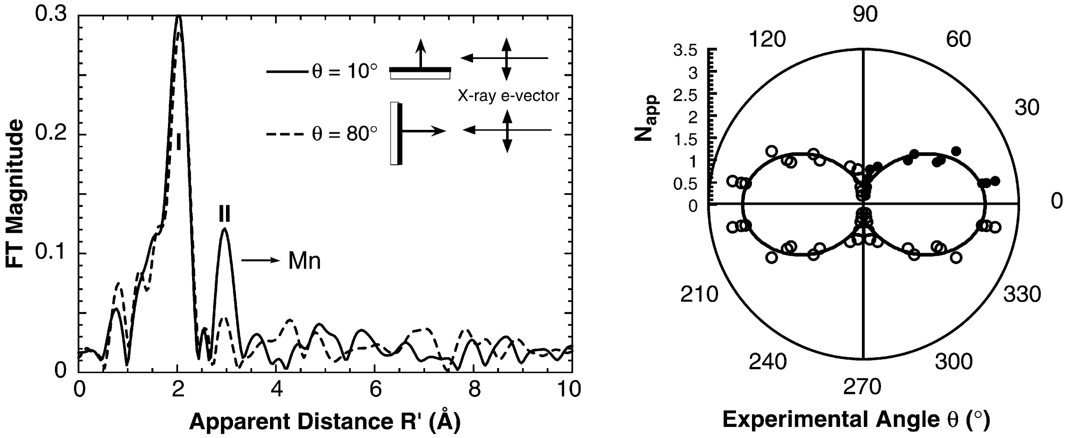

Fig. 10. Left. Fourier transforms of Sr-EXAFS from oriented Sr-PS II samples at two angles (θ). The dichroism is most readily apparent in Fourier peak II (R′ = 3.0 Å) which is assigned to backscattering from Mn. *Right.* The polar plot shows N_{exp} (filled circles) plotted vs. the angle of detection, θ. The solid line is the best fit from which we obtain N_{iso} (number of Mn neighbors to Sr is ~2) and ϕ (~23°), the angle the Mn-Sr vector makes with the membrane normal.

binding site of the native cofactor for any nearby Mn, within ~ 4 Å. The use of Ca EXAFS spectroscopy has produced results essentially congruent with those found by other independent methods: Sr EXAFS on Sr-reactivated PS II (Cinco et al., 1998) and Mn EXAFS on similar samples (Latimer et al., 1995), but it focuses on the native cofactor and avoids the treatments involving Ca depletion and Sr substitution. Like the earlier Sr EXAFS, the Ca EXAFS study has focused on the Ca cofactor of PS II (poised in the S_1 state). This technique is a more sensitive and direct probe of the Ca binding site in PS II and the Ca EXAFS experiment directly probed the Ca cofactor in as close to a native system as possible.

The FT of the Ca EXAFS is shown in Fig. 9, *Bottom* and the spectra are remarkably similar to the Fourier transforms of the earlier Sr EXAFS study with Sr substituted for Ca. The first (largest) Fourier peak corresponds to the coordinating oxygen atoms closest to Ca. In contrast to the control (NH_2OH-treated) sample, the Chelex-treated PS II shows a second Fourier peak. When Fourier peak II is isolated and simulated with possible scattering atoms, it corresponded best to Mn at 3.4 Å, rather than to light atom (C, O or Cl) neighbors. These results were consistent with the earlier Sr EXAFS studies.

The results are summarized in a motif shown in Fig. 11 and this motif depicts the Ca linked to two Mn by single-O bridges, which can be supplied by protein residues or water. Only single-oxygen bridges (not bidentate bridges) can provide the required 3.4 Å distance indicated by the Ca EXAFS fitting. This bridge may be derived from carboxylate ligands (aspartate or glutamate protein residues), protein backbone carboxyl, water or hydroxide.

Because significant information about Mn–Mn and Mn–Ca vector angles is now available, topological models previously discussed can be refined to include the presence of Ca and account for the dichroism data (Fig. 11). We have chosen to modify two options: option **F** (from Fig. 5) where the two di-μ-oxo motifs are formed using a common Mn atom and the mono-μ-oxo motif is placed at the end of the trinuclear unit, and option **G** can be thought of as at the corners of the base of a trigonal pyramid, with an O atom at the apex and three additional O atoms forming bridges pairwise among the Mn atoms below the base with the fourth Mn linked to one of the corner Mn atoms by a single O-atom bridge. Option **F** has two 2.7 to 2.8 Å Mn-Mn vectors while **G** has three such vectors. These structures are consistent with simulations of EPR and ENDOR data and also qualitatively in agreement with the reported electron density of the Mn cluster, especially the first option for **G** with Ca.

It has been speculated that Ca controls substrate water binding to the catalytic Mn site (Chen et al., 1995) and recent mechanisms have suggested the

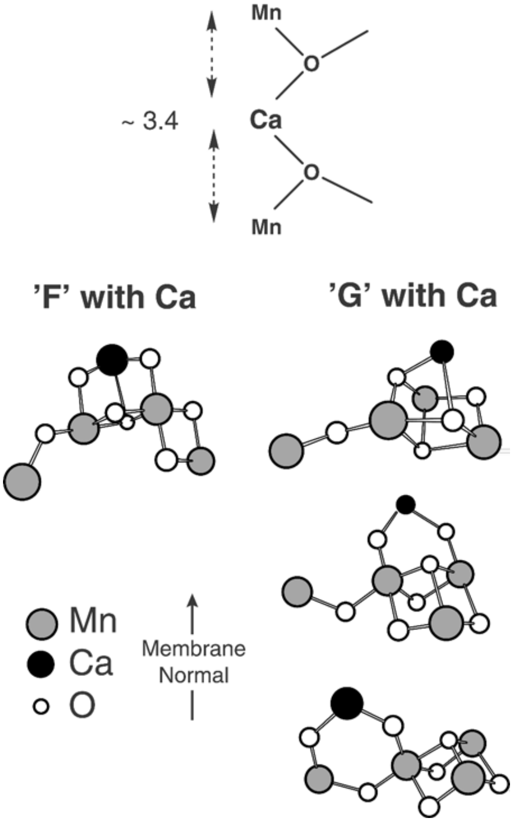

Fig. 11. Top. Model of Ca-binding site of the oxygen-evolving complex in PS II. From the results of the Ca EXAFS studies on PS II, the Ca cofactor is linked by two single-O bridges to two Mn. The oxygens can be provided by water, hydroxyl or protein residues (carboxylate, phenolate). Other ligands to Ca are not shown. The arrangement shown here is not unique as other placements of the two Mn around the Ca are conceivable (Cinco et al., 2002). *Bottom.* Refined models for the active site of the OEC in PS II. These models combine the finding from oriented Sr-substituted PS II samples with previous results from Mn EXAFS on oriented PS II samples. These are derived from core structures that have been described in earlier studies and the models presented here are based on options **F** and **G** from Fig. 5 (**F** with Ca is a variation on a model originally proposed by Siegbahn, 2000).

crucial involvement of the cofactor (Ananyev and Dismukes, 1997; Renger, 1997; Limburg et al., 1999; Siegbahn, 2000). The results Mn EXAFS, Sr EXAFS and Ca EXAFS are mutually consistent and converge toward the conclusion that the Ca cofactor is intimately structurally linked with the Mn cluster in PS II. Taken together, the three methods offer compelling evidence that the catalytic center of photosynthetic O_2 evolution is a heteronuclear Mn_4Ca cluster (for further details, see Chapter 21, Barber and Iwata).

V. Structural Role of the Chloride Cofactor

Despite a multitude of spectroscopic studies, definitive structural evidence for Mn-Cl ligation has not yet been reported. There is one functional Cl^- per PS II unit (Lindberg and Andréasson, 1996; Olesen and Andréasson, 2003), but it is unclear whether chloride is a ligand to one of the Mn atoms in any of the S-states (Lindberg et al., 1990). Steady-state kinetic studies indicate the presence of a halide binding site on the Mn complex (Sandusky and Yocum, 1986; Yocum, 1992; Lindberg and Andréasson, 1996) and activity is inhibited by some compounds which compete with the Cl^- binding site, such as fluoride (Sandusky and Yocum, 1986), primary amines (Sandusky and Yocum, 1986) and acetate (Clemens et al., 2002). Ono et al. (1986) have shown that Cl^- depleted PS II particles in the S_2 state do not have the usual multiline EPR signal but rather have a signal at g=4.1, signifying that an alternative S_2 state is formed. A similar EPR signal is observed on treatment with F^-. It was found that when the OEC is in this alternative state, it can no longer advance to higher S-states. However, the EPR multiline signal is restored following illumination and subsequent addition of Cl^-. Recent studies indicate that the presence of the Cl^- is necessary only for the S_2 to S_3 and S_3 to S_0 transitions of the OEC, while the earlier steps of the cycle can proceed in its absence (Wincencjusz et al., 1997, 1998). These studies indicate that Cl^- is closely associated with the structure of the OEC and the mechanism of O_2 evolution, but its detailed role is as yet unclear.

F^- perturbation of the Mn–Mn distances by treatment with F^- is one of the most direct structural data available that implies halide as a ligand of Mn. XAS studies of F^- inhibited samples show that one of the two 2.7 Å Mn–Mn distances is increased to ~2.8 Å, which is suggestive of F^- binding to the Mn cluster (DeRose et al., 1995). The recent ESEEM results from acetate treated PS II samples (Clemens et al., 2002) also provide the most direct spectroscopic evidence to date for the presence of a chloride ligand to Mn.

There is evidence from EXAFS studies with oriented S_3 state samples indicating the presence of Mn-Cl ligation in the S_3 state (Fernandez et al., 1998). EXAFS results from isotropic samples in the S_3 state have shown that there is considerable change

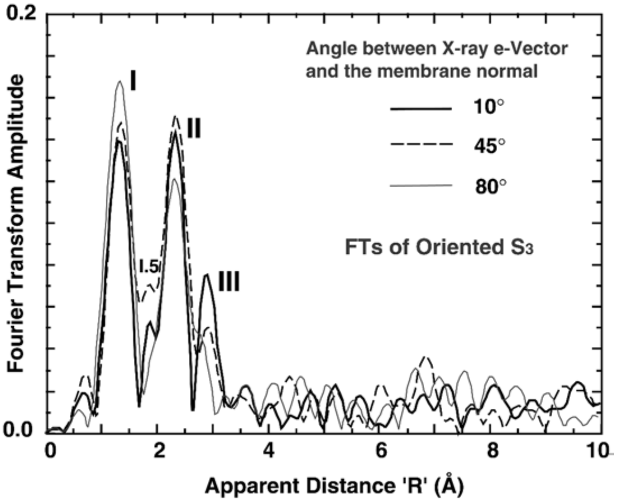

Fig. 12. The Fourier transform of an oriented S_3 sample. The Mn-Mn vectors represented by Fourier peaks labeled II and III are dichroic. Interestingly, a Fourier peak labeled 1.5 is discernible that is not observed in other S-states and it fits best to Cl, indicating the possible presence of a Cl ligand to Mn at a distance of 2.2 Å (Fernandez et al., 1998) in the S_3 state.

in the Mn–Mn distances as the system advances from the S_2 to the S_3 state (Liang et al., 2000). The two 2.7 Å Mn–Mn distances in the S_2 state increase to ~2.8 and ~3.0 Å in the S_3 state. With the aim of determining the relative orientation of the 2.8 and 2.9–3.0 Å Mn–Mn vectors, we initiated XAS studies of oriented S_3 state samples. The FT in Fig. 12 shows that the two Mn–Mn vectors are dichroic. Interestingly, maybe because of the lengthening of the Mn–Mn vectors, a new Fourier peak is observed between the first and second Fourier peaks, labeled 1.5 in Fig. 12. Comparing this FT with that of a Mn binuclear complex with one Cl^- as a terminal ligand to a Mn atom shows that the peak corresponding to Cl backscattering in the model complex is found at approximately the same apparent distance as the new Fourier peak in the PS II samples (Fernandez et al., 1998). In other model compounds, the amplitude of this peak increases as the ratio of Cl/Mn increases and the peak is absent when Cl^- is not present as a ligand. In the S_3 state sample, this peak does not fit to lower Z atoms such as C, N, or O. The fit is significantly better for Cl backscattering at ~2.2 Å. The fits for the model compound are very similar. Dichroism studies on S_3 state samples show that the Fourier peak is larger at the 10° orientation compared to the 80° orientation, which suggests that the Mn–Cl vector is more parallel to the membrane normal.

VI. Mechanism of Water Oxidation and O_2 Evolution

The mechanisms for water oxidation and oxygen evolution that have been proposed can be broadly divided into four categories in which the character of the oxygen atoms that ultimately form dioxygen is different. In these four groups the oxygen atoms come from: two terminal oxygens bound to two separate Mn atoms, one terminal oxygen and one oxygen not bound to the Mn cluster, one terminal and one bridging oxygen, or two μ-oxo bridges. Each of these mechanisms involves distinctly different Mn–O bonds formed and broken during the catalytic cycle (see Chapter 25 for details).

The contribution of X-ray studies to the mechanism of O_2 evolution is in resolving whether an oxygen atom derived from a bridging position in the Mn cluster is involved in the ultimate formation of dioxygen and in the determination of whether Mn centered oxidation occurs during each stage of the S-state transitions. Our X-ray spectra are strongly supportive of Mn cluster oxidation during the $S_0 \rightarrow S_1$ and $S_1 \rightarrow S_2$ transitions, they do not support a similar Mn-centered oxidation during $S_2 \rightarrow S_3$. Furthermore, EXAFS analyses show clear evidence of non-degeneracy in the three 2.7 Å vector lengths in S_0 and S_3, but not in S_1 and S_2, and shows significant structural change

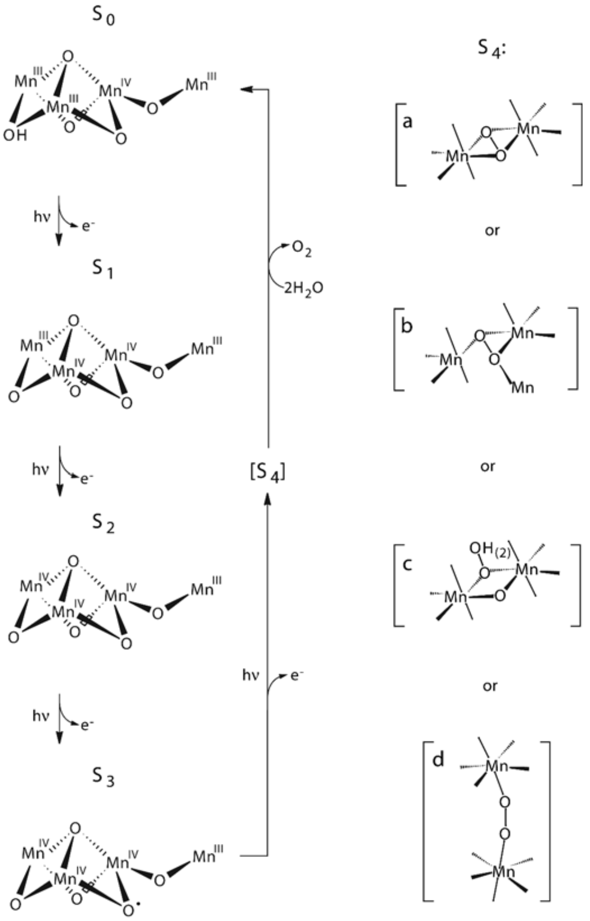

Fig. 13. Summary of changes in Mn oxidation states and Mn-Mn distances during photosynthetic water oxidation using option **G** in Fig. 5. In the $S_1 \rightarrow S_2$ transition, one Mn(III) is oxidized to Mn(IV), and the Mn–Mn distances do not change. During the $S_2 \rightarrow S_3$ transition, the oxidizing equivalent is localized on the μ-oxo bridge, which triggers the increase in Mn–Mn distances. In the $S_3 \rightarrow [S_4] \rightarrow S_0$ transition, a short-lived peroxo intermediate might be formed in the S_4 state. (a), (b), (c) and (d) are 4 mechanisms for O-O bond formation in the S_4 state. Mechanisms (a), (b) and (c) are where one or two bridging O atoms are directly involved in O-O bond formation; a motif that is consistent with XAS data. Mechanism (d) would require localization of an oxidizing equivalent on an oxo bridge that later exchanges or rearranges to a terminal O ligand before O-O bond formation. During the $S_0 \rightarrow S_1$ transition, a Mn(II) → Mn(III) oxidation or a Mn(III) to Mn(IV) concurrent with a deprotonation of a hydroxy to an oxo causing the decrease of the Mn–Mn distance is indicated. For clarity, Y_Z, the cofactors Ca^{2+} and Cl^-, and terminal Mn ligands are not shown. Mn–Mn distances were determined by EXAFS spectroscopy. As mentioned in DeRose et al. (1994), Cinco et al. (2002) and Robblee et al. (2002) other possible topological models exist for the OEC; similar mechanisms that can be proposed for each of the alternative topological models should be considered equally viable.

during the S_2 to S_3 transition that is not accompanied by a Mn-centered oxidation. The X-ray spectroscopy evidence supports the involvement of a bridging O atom in the mechanism of the formation of the O-O bond. These observations must be considered in any postulation of mechanistic aspects of the successive steps in water oxidation.

Our proposed mechanism (illustrated in Fig. 13 using the proposed model **G**) where the O-O bond is formed between one critical bridging oxygen and another oxygen atom derived from a bridging/terminal oxygen ligand or an exogenous oxygen also avoids the formation of the O–O bond until the most oxidized state (S_4) is reached (Fig. 13, (a), (b), (c)). All four options for the S_4 state generate O_2 which is derived from inequivalent oxygen atoms in the S_3 state, as shown by $^{16}O/^{18}O$ water-exchange measurements on the S_3 state (Messinger et al., 1995; Hillier et al., 1998). In addition, a recent $H_2{}^{16}O/H_2{}^{18}O$ FTIR experiment has shown the presence of an exchangeable di-μ-oxo-bridge in the S_1 and S_2 states (Chu et al., 2000). This mechanism precludes the formation and release of peroxide or other oxidation products of water in the earlier S-states, thus preventing the system from 'short circuiting' and avoiding the risk of damaging the polypeptides of PS II.

Acknowledgments

This work was supported by the National Institutes of Health grant (GM 55302) and by the Director, Office of Science, Office of Basic Energy Sciences, Division of Energy Biosciences, United States Department of Energy under contract DE-AC03-76SF00098. I am grateful to every one of the very talented and motivated graduate students and postdocs, and many sabbatical visitors to the Calvin Lab that I have had the privilege to work with on the oxygen evolving complex over the last two decades and more; each and every one of them can recognize some aspect of the work presented here that they were responsible for and that has contributed to the present understanding of the Mn cluster in the OEC. Specifically, the contributions to the research presented in this article by Roehl Cinco, John Robblee, Johannes Messinger, Henk Visser, Uwe Bergmann, Pieter Glatzel, Carmen Fernandez, Elodie Anxolabéhère-Mallart, Shelly Pizarro, Karen McFarlane, Junko Yano, Steve Cramer and Ken Sauer is gratefully acknowledged. Mel Klein's profound influence and contributions to the EPR and X-ray spectroscopy research pervades the work presented in this chapter. I extend my thanks to our collaborators Profs. W. H. Armstrong, G. W. Brudvig, G. Christou, T. Collins, J.-J. Girerd, R. N. Mukherjee, V. L. Pecoraro and K. Wieghardt who have generously provided all the inorganic Mn compounds that has made all the difference in analyzing the data from PS II. Synchrotron radiation facilities were provided by the Stanford Synchrotron Radiation Laboratory (SSRL) and the Advanced Photon Source (APS), both supported by the United States Department of Energy and the National Institutes of Health.

References

Adelroth P, Lindberg K and Andréasson LE (1995) Studies of Ca^{2+} binding in spinach Photosystem II using $^{45}Ca^{2+}$. Biochemistry 34: 9021–9027

Åhrling KA, Peterson S and Styring S (1998) The S_0 state EPR signal from the Mn cluster in Photosystem II arises from an isolated S=½ ground state. Biochemistry 37: 8115–8120

Ananyev GM and Dismukes GC (1997) Calcium induces binding and formation of a spin-coupled dimanganese (II, II) center in the apo-water oxidation complex of Photosystem II as precursor to the functional tetra-Mn/Ca cluster. Biochemistry 36: 11342–11350

Auger N, Girerd J-J, Corbella M, Gleizes A and Zimmermann J-L (1990) Synthesis, structure, and magnetic properties of the stable triangular $[Mn(IV)_3O_4]^{4+}$ core. J Am Chem Soc 112: 448–450

Beck WF, Depaula JC and Brudvig GW (1986) Ammonia binds to the manganese site of the O_2-evolving complex of Photosystem-II in the S_2 state. J Am Chem Soc 108: 4018–4022

Bergmann U, Grush MM, Horne CR, DeMarois P, Penner-Hahn JE, Yocum CF, Wright DW, Dubé CE, Armstrong WH, Christou G, Eppley HJ and Cramer SP (1998) Characterization of the Mn oxidation states in Photosystem II by Kβ X-ray fluorescence spectroscopy. J Phys Chem B 102: 8350–8352

Boussac A and Rutherford AW (1988a) S-state formation after Ca^{2+} depletion in the Photosystem II oxygen-evolving complex. Chem Script 28A: 123–126

Boussac A and Rutherford AW (1988b) Nature of the inhibition of the oxygen-evolving enzyme of Photosystem II induced by NaCl washing and reversed by the addition of Ca^{2+} or Sr^{2+}. Biochemistry 27: 3476–3483

Boussac A and Rutherford AW (2000) Comparative study of the g=4.1 EPR signals in the S_2 state of Photosystem II. Biochim Biophys Acta 1457: 145–156

Boussac A, Girerd J-J and Rutherford AW (1996) Conversion of the spin state of the manganese complex in Photosystem II induced by near-infrared light. Biochemistry 35: 6984–6989

Britt RD (1996) Oxygen evolution. In: Ort DR and Yocum CF (eds) Oxygenic Photosynthesis: The Light Reactions, pp 137–164. Kluwer Academic Publishers, Dordrecht

Britt RD, Zimmermann J-L, Sauer K and Klein MP (1989) Ammonia binds to the catalytic manganese of the oxygen-evolving complex of Photosystem II. Evidence by electron spin-echo envelope modulation spectroscopy. J Am Chem Soc 111: 3522–3532

Britt RD, Peloquin JM and Campbell KA (2000) Pulsed and parallel-polarization EPR characterization of the Photosystem II oxygen-evolving complex. Ann Rev Biophys Biomol Struct 29: 463–495

Cammarata KV and Cheniae GM (1987) Studies on 17, 24 kDa depleted Photosystem II membranes. Plant Physiol 84: 587–595

Carrell TG, Tyryshkin AM and Dismukes GC (2002) An evaluation of structural models for the photosynthetic water-oxidizing complex derived from spectroscopic and X-ray diffraction signatures. J Biol Inorg Chem 7: 2–22

Chen C, Kazimir J and Cheniae GM (1995) Calcium modulates the photoassembly of Photosystem II $(Mn)_4$-clusters by preventing ligation of nonfunctional high-valency states of manganese. Biochemistry 34: 13511–13526

Chu H-A, Sackett H and Babcock GT (2000) Identification of a Mn-O-Mn cluster vibrational mode of the oxygen-evolving complex in Photosystem II by low-frequency FTIR spectroscopy. Biochemistry 39: 14371–14376

Cinco RM, Robblee JH, Rompel A, Fernandez C, Yachandra VK, Sauer K and Klein MP (1998) Strontium EXAFS reveals the proximity of calcium to the manganese cluster of oxygen-evolving Photosystem II. J Phys Chem B 102: 8248–8256

Cinco RM, Rompel A, Visser H, Aromí G, Christou G, Sauer K, Klein MP and Yachandra VK (1999) Comparison of the manganese cluster in oxygen-evolving Photosystem II with distorted cubane manganese compounds through X-ray absorption spectroscopy. Inorg Chem 38: 5988–5998

Cinco RM, Holman KLM, Robblee JH, Yano J, Pizarro SA, Bellacchio E, Sauer K and Yachandra VK (2002) Calcium EXAFS establishes the Mn-Ca cluster in the oxygen-evolving complex of Photosystem II. Biochemistry 41: 12928–12933

Clemens KL, Force DA and Britt RD (2002) Acetate binding at the Photosystem II oxygen evolving complex: An S_2-state multiline signal ESEEM study. J Am Chem Soc 124: 10921–10933

Cole J, Yachandra VK, Guiles RD, McDermott AE, Britt RD, Dexheimer SL, Sauer K and Klein MP (1987) Assignment of the $g = 4.1$ EPR signal to manganese in the S_2 state of the photosynthetic oxygen-evolving complex: An X-ray absorption edge spectroscopy study. Biochim Biophys Acta 890: 395–398

Cramer SP (1988) Biochemical application of X-ray absorption spectroscopy. In: Koningsberger DC and Prins R (eds) X-Ray Absorption: Principles, Applications, Techniques of EXAFS, SEXAFS and XANES, pp 327–320. John Wiley & Sons, New York

Dau H, Andrews JC, Roelofs TA, Latimer MJ, Liang W, Yachandra VK, Sauer K and Klein MP (1995) Structural consequences of ammonia binding to the manganese cluster of the photosynthetic oxygen-evolving complex: An X-ray absorption study of isotropic and oriented Photosystem II particles. Biochemistry 34: 5274–5287

Debus RJ (1992) The manganese and calcium ions of photosynthetic oxygen evolution. Biochim Biophys Acta 1102: 269–352

Dekker JP (1992) Optical studies on the oxygen-evolving complex of Photosystem II. In: Pecoraro VL (ed) Manganese Redox Enzymes, pp 85–103. VCH Publishers, New York

DeRose VJ, Mukerji I, Latimer MJ, Yachandra VK, Sauer K and Klein MP (1994) Comparison of the manganese oxygen-evolving complex in Photosystem II of spinach and *Synechococcus* sp. with multinuclear manganese model compounds by X-ray absorption spectroscopy. J Am Chem Soc 116: 5239–5249

DeRose VJ, Latimer MJ, Zimmermann J-L, Mukerji I, Yachandra VK, Sauer K and Klein MP (1995) Fluoride substitution in the Mn cluster from Photosystem II: EPR and X-ray absorption spectroscopy studies. Chem Phys 194: 443–459

Dismukes GC and Siderer Y (1981) Intermediates of a polynuclear manganese cluster involved in photosynthetic oxidation of water. Proc Natl Acad Sci USA 78: 274–278

Evelo RG, Styring S, Rutherford AW and Hoff AJ (1989) EPR relaxation measurements of Photosystem-II reaction centers — influence of S-state oxidation and temperature. Biochim Biophys Acta 973: 428–442

Fernandez C, Cinco RM, Robblee JH, Messinger J, Pizarro SA, Sauer K, Klein MP and Yachandra VK (1998) Calcium and chloride cofactors of the oxygen evolving complex — X-ray absorption spectroscopy evidence for a Mn/Ca/Cl heteronuclear cluster. In: Garab G (ed) Photosynthesis: Mechanisms and Effects, Vol II, pp 1399–1402. Kluwer Academic Publishers, Dordrecht

Ferreira K, Iverson TM, Mughlouni K, Barber J and Iwata S (2004) Architecture of the photosynthetic oxygen-evolving center. Science 303: 1831–1838

George GN, Prince RC and Cramer SP (1989) The manganese site of the photosynthetic water-splitting enzyme. Science 243: 789–791

Ghanotakis DF, Babcock GT and Yocum CF (1984) Calcium reconstitutes high rates of oxygen evolution in polypeptide depleted Photosystem II preparations. FEBS Lett 167: 127–130

Ghanotakis DF, Babcock GT and Yocum CF (1985) Structure of the oxygen-evolving complex of Photosystem II: Calcium and lanthanum compete for sites on the oxidizing side of Photosystem II which control the binding of water-soluble polypeptides and regulate the activity of the manganese complex. Biochim Biophys Acta 809: 173–180

Gilchrist ML, Jr., Ball JA, Randall DW and Britt RD (1995) Proximity of the manganese cluster of Photosystem II to the redox-active tyrosine Y_Z. Proc Natl Acad Sci USA 92: 9545–9549

Goodin DB, Yachandra VK, Britt RD, Sauer K and Klein MP (1984) The state of manganese in the photosynthetic apparatus. 3. Light-induced changes in X-ray absorption (K-edge) energies of manganese in photosynthetic membranes. Biochim Biophys Acta 767: 209–216

Guiles RD, Yachandra VK, McDermott AE, Cole JL, Dexheimer SL, Britt RD, Sauer K and Klein MP (1990a) The S_0 state of Photosystem II induced by hydroxylamine: Differences between the structure of the manganese complex in the S_0 and S_1 states determined by X-ray absorption spectroscopy. Biochemistry 29: 486–496

Guiles RD, Zimmermann JL, McDermott AE, Yachandra VK, Cole JL, Dexheimer SL, Britt RD, Wieghardt K, Bossek U, Sauer K and Klein MP (1990b) The S_3 state of Photosystem II: Differences between the structure of the manganese complex in the S_2 and S_3 states determined by X-ray absorption-spectroscopy. Biochemistry 29: 471–485

Han K-C and Katoh S (1993) Different localization of two Ca^{2+} in spinach oxygen-evolving Photosystem II membranes. Evidence for involvement of only one Ca^{2+} in oxygen evolution. Plant Cell Physiol 34: 585–593

Hasegawa K, Kusunoki M, Inoue Y and Ono T-A (1998) Simulation of S_2-state multiline EPR signal in oriented Photosystem II membranes: Structural implications for the manganese cluster in an oxygen-evolving complex. Biochemistry 37: 9457–9465

Hasegawa K, Ono T-A, Inoue Y and Kusunoki M (1999) Spin-exchange interactions in the S_2-state manganese tetramer in photosynthetic oxygen-evolving complex deduced from g=2 multiline EPR signal. Chem Phys Lett 300: 9–19

Hillier W, Messinger J and Wydrzynski T (1998) Kinetic determination of the fast exchanging substrate water molecule in the S_3 state of Photosystem II. Biochemistry 37: 16908–16914

Iuzzolino L, Dittmer J, Dörner W, Meyer-Klaucke W and Dau H (1998) X-ray absorption spectroscopy on layered Photosystem II membrane particles suggests manganese-centered oxidation of the oxygen-evolving complex for the S_0-S_1, S_1-S_2, and S_2-S_3 transitions of the water oxidation cycle. Biochemistry 37: 17112–17119

Jaklevic J, Kirby JA, Klein MP, Robertson AS, Brown GS and

Eisenberger P (1977) Fluorescence detection of EXAFS: Sensitivity enhancement for dilute species and thin films. Solid State Commun 23: 679–682

Joliot P (2003) Period-four oscillations of the flash-induced oxygen formation in photosynthesis. Photosynth Res 76: 65–72

Kamiya N and Shen JR (2003) Crystal structure of oxygen-evolving Photosystem II from *Thermosynechococcus vulcanus* at 3.7 Å resolution. Proc Natl Acad Sci USA 100: 98–103

Katoh S, Satoh K, Ohno T, Chen J-R and Kashino Y (1987) Numbers of calcium ions associated with oxygen evolving Photosystem II preparations with different affinities. In: Biggins J (ed) Progress in Photosynthesis Research, Vol I, pp 625–628. Martinus Nijhoff Publishers, Dordrecht

Kirby JA, Robertson AS, Smith JP, Thompson AC, Cooper SR and Klein MP (1981) State of manganese in the photosynthetic apparatus. 1. Extended X-ray absorption fine structure studies on chloroplasts and di-μ-oxo-bridged dimanganese model compounds. J Am Chem Soc 103: 5529–5537

Kok B, Forbush B and McGloin M (1970) Cooperation of charges in photosynthetic oxygen evolution. I. A linear four step mechanism. Photochem Photobiol 11: 457–475

Kretschmann H, Dekker JP, Saygin Ö and Witt HT (1988) An agreement on the quaternary oscillation of ultraviolet absorption changes accompanying the water splitting in isolated Photosystem II complexes from the cyanobacterium *Synechococcus* sp. Biochim Biophys Acta 932: 358–361

Kusunoki M, Takano T, Ono T, Noguchi T, Yamaguchi Y, Oyanagi H and Inoue Y (1995) Advanced EXAFS studies of the S_1 state manganese cluster in plant Photosystem II. In: Mathis P (ed) Photosynthesis: From Light to Biosphere, Vol II, pp 251–254. Kluwer Academic Publishers, Dordrecht

Kuzek D and Pace RJ (2001) Probing the Mn oxidation states in the OEC Insights from spectroscopic, computational and kinetic data. Biochim Biophys Acta 1503: 123–137

Lakshmi KV, Eaton SS, Eaton GR, Frank HA and Brudvig GW (1998) Analysis of dipolar and exchange interactions between manganese and tyrosine Z in the $S_2Y_Z^{\bullet}$ state of acetate-inhibited Photosystem II via EPR spectral simulations at X- and Q-bands. J Phys Chem B 102: 8327–8335

Latimer MJ, DeRose VJ, Mukerji I, Yachandra VK, Sauer K and Klein MP (1995) Evidence for the proximity of calcium to the manganese cluster of Photosystem II: Determination by X-ray absorption spectroscopy. Biochemistry 34: 10898–10909

Latimer MJ, DeRose VJ, Yachandra VK, Sauer K and Klein MP (1998) Structural effects of calcium depletion on the manganese cluster of Photosystem II: Determination by X-ray absorption spectroscopy. J Phys Chem B 102: 8257–8265

Liang W, Latimer MJ, Dau H, Roelofs TA, Yachandra VK, Sauer K and Klein MP (1994) Correlation between structure and magnetic spin state of the manganese cluster in the oxygen-evolving complex of Photosystem II in the S_2 state: Determination by X-ray absorption spectroscopy. Biochemistry 33: 4923–4932

Liang W, Roelofs TA, Cinco RM, Rompel A, Latimer MJ, Yu WO, Sauer K, Klein MP and Yachandra VK (2000) Structural change of the Mn cluster during the $S_2 \rightarrow S_3$ state transition of the oxygen-evolving complex of Photosystem II. Does it reflect the onset of water/substrate oxidation? Determination by Mn X-ray absorption spectroscopy. J Am Chem Soc 122: 3399–3412

Limburg J, Szalai VA and Brudvig GW (1999) A mechanistic and structural model for the formation and reactivity of a Mn^{v}=O species in photosynthetic water oxidation. J Chem Soc, Dalton Trans 1353–1361

Lindberg K and Andréasson LE (1996) A one-site, two-state model for the binding of anions in Photosystem II. Biochemistry 35: 14259–14267

Lindberg K, Wydrzynski T, Vänngård T and Andréasson L-E (1990) Slow release of chloride from ^{36}Cl-labeled Photosystem II membranes. FEBS Lett 264: 153–155

MacLachlan DJ, Hallahan BJ, Ruffle SV, Nugent JHA, Evans MCW, Strange RW and Hasnain SS (1992) An EXAFS study of the manganese oxygen-evolving complex in purified Photosystem II membrane fractions. The S_1 and S_2 states. Biochem J 285: 569–576

MacLachlan DJ, Nugent JHA, Bratt PJ and Evans MCW (1994) The effects of calcium depletion on the O_2-evolving complex in spinach PS II: The S_1^*, S_2^* and S_3^* states and the role of the 17 kDa and 23 kDa extrinsic polypeptides. Biochim Biophys Acta 1186: 186–200

McDermott AE, Yachandra VK, Guiles RD, Cole JL, Dexheimer SL, Britt RD, Sauer K and Klein MP (1988) Characterization of the manganese O_2-evolving complex and the iron-quinone acceptor complex in Photosystem II from a thermophilic cyanobacterium by electron paramagnetic resonance and X-ray absorption spectroscopy. Biochemistry 27: 4021–4031

Messinger J, Badger M and Wydrzynski T (1995) Detection of *one* slowly exchanging substrate water molecule in the S_3 state of Photosystem II. Proc Natl Acad Sci USA 92: 3209–3213

Messinger J, Nugent JHA and Evans MCW (1997a) Detection of an EPR multiline signal for the S_0^* state in Photosystem II. Biochemistry 36: 11055–11060

Messinger J, Robblee J, Yu WO, Sauer K, Yachandra VK and Klein MP (1997b) The S_0 state of the oxygen-evolving complex in Photosystem II is paramagnetic: Detection of an EPR multiline signal. J Am Chem Soc 119: 11349–11350

Messinger J, Robblee JH, Bergmann U, Fernandez C, Glatzel P, Visser H, Cinco RM, McFarlane KL, Bellacchio E, Pizarro SA, Cramer SP, Sauer K, Klein MP and Yachandra VK (2001) Absence of Mn-centered oxidation in the $S_2 \rightarrow S_3$ transition: Implications for the mechanism of photosynthetic water oxidation. J Am Chem Soc 123: 7804–7820

Mukerji I, Andrews JC, DeRose VJ, Latimer MJ, Yachandra VK, Sauer K and Klein MP (1994) Orientation of the oxygen-evolving manganese complex in a Photosystem II membrane preparation: An X-ray absorption spectroscopy study. Biochemistry 33: 9712–9721

Olesen K and Andréasson LE (2003) The function of the chloride ion in photosynthetic oxygen evolution. Biochemistry 42: 2025–2035

Ono T-A and Inoue Y (1988) Discrete extraction of the Ca atom functional for O_2 evolution in higher plant Photosystem II by a simple low pH treatment. FEBS Lett 227: 147–152

Ono T-A and Inoue Y (1989) Roles of Ca^{2+} in O_2 evolution in higher plant Photosystem II: Effects of replacement of Ca^{2+} site by other cations. Arch Biochem Biophys 275: 440–448

Ono T-A, Zimmermann JL, Inoue Y and Rutherford AW (1986) EPR evidence for a modified S-state transition in chloride-depleted Photosystem II. Biochim Biophys Acta 851: 193–201

Ono T-A, Noguchi T, Inoue Y, Kusunoki M, Matsushita T and Oyanagi H (1992) X-ray detection of the period-four cycling of the manganese cluster in photosynthetic water oxidizing enzyme. Science 258: 1335–1337

Ono T-A, Noguchi T, Inoue Y, Kusunoki M, Yamaguchi H and Oyanagi H (1994) Study of the intermediate S-states for water oxidation in the normal and Ca-depleted photosynthetic oxygen-evolving enzyme by means of flash-induced X-ray absorption near edge structure spectroscopy. Biochem Soc Trans 22: 331-335

Pecoraro VL (ed) (1992) Manganese Redox Enzymes. VCH Publishers, New York

Pecoraro VL and Hsieh W-Y (2000) The use of model complexes to elucidate the structure and function of manganese redox enzymes. In: Sigel A and Sigel H (eds) Manganese and Its Role in Biological Processes, pp 429–504. Marcel Dekker Inc., New York

Peloquin JM and Britt RD (2001) EPR/ENDOR characterization of the physical and electronic structure of the OEC Mn cluster. Biochim Biophys Acta 1503: 96–111

Peloquin JM, Campbell KA and Britt RD (1998) ^{55}Mn pulsed ENDOR demonstrates that the Photosystem II ‘split’ EPR signal arises from a magnetically-coupled mangano-tyrosyl complex. J Am Chem Soc 120: 6840–6841

Peloquin JM, Campbell KA, Randall DW, Evanchik MA, Pecoraro VL, Armstrong WH and Britt RD (2000) ^{55}Mn ENDOR of the S_2-state multiline EPR signal of Photosystem II: Implications on the structure of the tetranuclear cluster. J Am Chem Soc 122: 10926–10942

Peng G, de Groot FMF, Hämäläinen K, Moore JA, Wang X, Grush MM, Hastings JB, Siddons DP, Armstrong WH, Mullins OC and Cramer SP (1994) High-resolution manganese X-ray fluorescence spectroscopy. Oxidation-state and spin-state sensitivity. J Am Chem Soc 116: 2914–2920

Penner-Hahn JE (1998) Structural characterization of the Mn site in the photosynthetic oxygen-evolving complex. Struct Bond 90: 1–36

Penner-Hahn JE, Fronko RM, Pecoraro VL, Yocum CF, Betts SD and Bowlby NR (1990) Structural characterization of the manganese sites in the photosynthetic oxygen-evolving complex using X-ray absorption- spectroscopy. J Am Chem Soc 112: 2549–2557

Renger G (1997) Mechanistic and structural aspects of photosynthetic water oxidation. Physiol Plant 100: 828–841

Riggs PJ, Yocum CF, Penner-Hahn JE and Mei R (1992) Reduced derivatives of the manganese cluster in the photosynthetic oxygen-evolving complex. J Am Chem Soc 114: 10650–10651

Riggs-Gelasco PJ, Mei R, Yocum CF and Penner-Hahn JE (1996a) Reduced derivatives of the Mn cluster in the oxygen-evolving complex of Photosystem II: An EXAFS study. J Am Chem Soc 118: 2387–2399

Riggs-Gelasco PJ, Mei R, Ghanotakis DF, Yocum CF and Penner-Hahn JE (1996b) X-ray absorption spectroscopy of calcium-substituted derivatives of the oxygen-evolving complex of Photosystem II. J Am Chem Soc 118: 2400–2410

Robblee JH, Cinco RM and Yachandra VK (2001) X-ray spectroscopy-based structure of the Mn cluster and mechanism of photosynthetic oxygen evolution. Biochim Biophys Acta 1503: 7–23

Robblee JH, Messinger J, Cinco RM, McFarlane KL, Fernandez C, Pizarro SA, Sauer K and Yachandra VK (2002) The Mn cluster in the S_0 state of the oxygen-evolving complex of Photosystem II studied by EXAFS spectroscopy: Are there three di-μ-oxo-bridged Mn_2 moieties in the tetranuclear Mn complex? J Am Chem Soc 124: 7459–7471

Roe AL, Schneider DJ, Mayer RJ, Pyrz JW, Widom J and Que L, Jr (1984) X-ray absorption spectroscopy of iron-tyrosinate proteins. J Am Chem Soc 106: 1676–1681

Roelofs TA, Liang W, Latimer MJ, Cinco RM, Rompel A, Andrews JC, Sauer K, Yachandra VK and Klein M (1996) Oxidation states of the manganese cluster during the flash-induced S-state cycle of the photosynthetic oxygen-evolving complex. Proc Natl Acad Sci USA 93: 3335–3340

Rutherford AW, Zimmermann J-L and Boussac A (1992) Oxygen evolution. In: Barber J (ed) The Photosystems: Structure, Function, and Molecular Biology, pp 179–229. Elsevier Science Publishers BV, Amsterdam

Sandusky PO and Yocum CF (1986) The chloride requirement for photosynthetic oxygen evolution: Factors affecting nucleophilic displacement of chloride from the oxygen-evolving complex. Biochim Biophys Acta 849: 85–93

Sauer K, Yachandra VK, Britt RD and Klein MP (1992) The photosynthetic water oxidation complex studied by EPR and X-ray absorption spectroscopy. In: Pecoraro VL (ed) Manganese Redox Enzymes, pp 141–175. VCH Publishers, New York

Sayers DE, Stern EA and Lytle F (1971) New technique for investigating noncrystalline structures. Fourier analysis of the extended X-ray-absorption fine structure. Phys Rev Lett 27: 1204–1207

Saygin Ö and Witt HT (1987) Optical characterization of intermediates in the water-splitting enzyme system of photosynthesis—possible states and configurations of manganese and water. Biochim Biophys Acta 893: 452–469

Schiller H, Dittmer J, Iuzzolino L, Dörner W, Meyer-Klaucke W, Solé VA, Nolting H-F and Dau H (1998) Structure and orientation of the oxygen-evolving manganese complex of green algae and higher plants investigated by X-ray absorption linear dichroism spectroscopy on oriented Photosystem II membrane particles. Biochemistry: 37: 7340–7350

Sharp RR (1992) Proton NMR relaxation due to the photosynthetic oxygen-evolving center. In: Pecoraro VL (ed) Manganese Redox Enzymes, pp 177–196. VCH Publishers, New York

Shen J-R, Satoh K and Katoh S (1988) Calcium content of oxygen-evolving Photosystem II preparations from higher plants. Effects of NaCl treatment. Biochim Biophys Acta 933: 358–364

Shulman RG, Yafet Y, Eisenberger P and Blumberg WE (1976) Observation and interpretation of X-ray absorption edges in iron compounds and proteins. Proc Natl Acad Sci USA 73: 1384–1388

Siegbahn PEM (2000) Theoretical models for the oxygen radical mechanism of water oxidation and of the water oxidizing complex of Photosystem II. Inorg Chem 39: 2923–2935

Sivaraja M, Tso J and Dismukes GC (1989) A calcium-specific site influences the structure and activity of the manganese cluster responsible for photosynthetic water oxidation. Biochemistry 28: 9459–9464

Smith PJ and Pace RJ (1996) Evidence for two forms of the g=4.1 signal in the S_2 state of Photosystem II. Two magnetically isolated manganese dimers. Biochim Biophys Acta 1275: 213–220

Styring SA and Rutherford AW (1988) The microwave power saturation of S_{IIslow} varies with the redox state of the oxygen-evolving complex in Photosystem II. Biochemistry 27: 4915–4923

Tamura N and Cheniae G (1985) Effects of Photosystem-II extrinsic proteins on microstructure of the oxygen-evolving complex and its reactivity to water analogs. Biochim Biophys Acta 809: 245–259

Tsutsumi K, Nakamori H and Ichikawa K (1976) X-ray manganese Kβ emission spectra of manganese oxides and manganates. Phys Rev B 13: 929–933

Visser H, Anxolabéhère-Mallart E, Bergman U, Glatzel P, Robblee JH, Cramer SP, Girerd J-J, Sauer K, Klein MP and Yachandra VK (2001) Mn K-edge XANES and Kβ XES studies of two Mn-oxo binuclear complexes. Investigation of three different oxidation states relevant to the oxygen-evolving complex of Photosystem II. J Am Chem Soc 123: 7031–7039

Westre TE, Kennepohl P, DeWitt JG, Hedman B, Hodgson KO and Solomon EI (1997) A multiplet analysis of Fe K-edge 1s to 3d pre-edge features of iron complexes. J Am Chem Soc 119: 6297–6314

Wieghardt K (1989) The active centers in manganese-containing metalloproteins and inorganic model complexes. Angew Chem Int Ed Engl 28: 1153–1172

Wincencjusz H, van Gorkom HJ and Yocum CF (1997) The photosynthetic oxygen evolving complex requires chloride for its redox state S_2 to S_3 and S_3 to S_0 transitions but not for S_0 to S_1 or S_1 to S_2 transitions. Biochemistry 36: 3663–3670

Wincencjusz H, Yocum CF and van Gorkom HJ (1998) S-state dependence of chloride binding affinities and exchange dynamics in the intact and polypeptide-depleted O_2 evolving complex of Photosystem II. Biochemistry 37: 8595–8604

Yachandra VK (1995) X-ray absorption spectroscopy and applications in structural biology. In: Sauer K (ed) Methods of Enzymology, Vol 246, pp 638–675. Academic Press, San Diego

Yachandra VK (2002) Structure of the manganese complex in Photosystem II: Insights from X-ray spectroscopy. Phil Trans R Soc London B 357: 1347–1357

Yachandra VK, Guiles RD, McDermott A, Britt RD, Dexheimer SL, Sauer K and Klein MP (1986) The state of manganese in the photosynthetic apparatus. 4. Structure of the manganese complex in Photosystem II studied using EXAFS spectroscopy. The S_1 state of the oxygen-evolving Photosystem II complex from spinach. Biochim Biophys Acta 850: 324–332

Yachandra VK, Guiles RD, McDermott AE, Cole JL, Britt RD, Dexheimer SL, Sauer K and Klein MP (1987) Comparison of the structure of the manganese complex in the S_1 and S_2 states of the photosynthetic O_2-evolving complex: An X-ray absorption spectroscopy study. Biochemistry 26: 5974–5981

Yachandra VK, DeRose VJ, Latimer MJ, Mukerji I, Sauer K and Klein MP (1993) Where plants make oxygen: A structural model for the photosynthetic oxygen-evolving manganese cluster. Science 260: 675–679

Yachandra VK, Sauer K and Klein MP (1996) Manganese cluster in photosynthesis: Where plants oxidize water to dioxygen. Chem Rev 96: 2927–2950

Yocum CF (1992) The calcium and chloride requirements for photosynthetic water oxidation. In: Pecoraro VL (ed) Manganese Redox Enzymes, pp 71–84. VCH Publishers, New York

Zheng M and Dismukes GC (1996) Orbital configuration of the valence electrons, ligand field symmetry, and manganese oxidation states of the photosynthetic water oxidizing complex: Analysis of the S_2 state multiline EPR signals. Inorg Chem 35: 3307–3319

Zimmermann JL and Rutherford AW (1986) Electron paramagnetic resonance properties of the S_2 state of the oxygen-evolving complex of Photosystem II. Biochemistry 25: 4609–4615

Zouni A, Witt HT, Kern J, Fromme P, Krauss N, Saenger W and Orth P (2001) Crystal structure of Photosystem II from *Synechococcus elongatus* at 3.8 Å resolution. Nature 409: 739–743